HHS Public Access

Author manuscript

Nature. Author manuscript; available in PMC 2018 March 07.

Published in final edited form as:

Nature. 2017 December 14; 552(7684): 273–277. doi:10.1038/nature25003.

KAT2A coupled with the α-KGDH complex acts as a histone H3 succinyltransferase

Yugang Wang[1,*], **Yusong R. Guo**[2,*], **Ke Liu**[3], **Zheng Yin**[4], **Rui Liu**[1], **Yan Xia**[1], **Lin Tan**[5], **Peiying Yang**[5], **Jong-Ho Lee**[1], **Xin-jian Li**[1], **David Hawke**[6], **Yanhua Zheng**[1], **Xu Qian**[7], **Jianxin Lyu**[7,8], **Jie He**[9], **Dongming Xing**[10,11,12,§], **Yizhi Jane Tao**[2,§], and **Zhimin Lu**[1,13,14,§]

[1]Brain Tumor Center, Department of Neuro-Oncology, The University of Texas MD Anderson Cancer Center, Houston, Texas 77030, USA

[2]Department of BioSciences, Rice University, Houston, Texas 77005, USA

[3]Department of Statistics, University of California, Berkeley, California 94720, USA

[4]Department of Systems Medicine and Bioengineering, Houston Methodist Research Institute, Houston, Texas 77030, USA

[5]Department of General Oncology, Division of Cancer Medicine, The University of Texas MD Anderson Cancer Center, Houston, Texas 77054, USA

[6]Department of Molecular Pathology, The University of Texas MD Anderson Cancer Center, Houston, Texas 77030, USA

[7]People's Hospital of Hangzhou Medical College, Hangzhou, Zhejiang 310014, China

[8]Key Laboratory of Laboratory Medicine, Ministry of Education of China, School of Laboratory Medicine and Life Science, Wenzhou Medical University, Wenzhou, Zhejiang 325035, China

[9]Laboratory of Thoracic Surgery, Cancer Institute and Hospital, Chinese Academy of Medical Sciences, Peking Union Medical College, Beijing 100021, China

[10]Cancer Institute, The Affiliated Hospital of Qingdao University, Qingdao, Shandong 266061, China

---

Correspondence and requests for materials should be addressed to Z.L. (zhiminlu@mdanderson.org), Y.J.T. (ytao@rice.edu) or D.X. (pharm@mail.tsinghua.edu.cn).

*These authors contributed equally to this work.

§These authors jointly supervised this work.

Supplementary Information is available in the online version of the paper.

Online Content Methods, along with any additional Extended Data display items and Source Data, are available in the online version of the paper; references unique to these sections appear only in the online paper.

The authors declare no competing financial interests.

Readers are welcome to comment on the online version of the paper.

Author Contributions Z.L., Y.J.T., D.X., and Y.W. conceived and designed the study and wrote the manuscript. Y.W., R.L., Y.X., Y.Z., and J.L. performed the biochemistry experiments to identify the succinyltransferase activity of KAT2A. Y.R.G., Y.W., and Y.J.T. generated co-crystal structures of KAT2A and Co-enzyme A analogues. Z.Y. and K.L. performed bioinformatics analyses. L.T. and P.Y. performed quantification analyses of acetyl-CoA and succinyl-CoA in cells. X.L. identified the nuclear localization sequence on DLST. X.Q. performed animal tissue studies. D.H. identified KAT2A-mediated histone H3 succinylation residue. P.Y., J.-H.L., D.X., J.L., and J.H. provided technical support.

[11]Qingdao Cancer Institute, Qingdao, Shandong 266061, China

[12]School of Life Sciences, Tsinghua University, Beijing, 100084, China

[13]Department of Molecular and Cellular Oncology, The University of Texas MD Anderson Cancer Center, Houston, Texas 77030, USA

[14]MD Anderson Cancer Center UTHealth Graduate School of Biomedical Sciences, The University of Texas, Houston, Texas 77030, USA

Abstract

Histone modifications, such as the frequently occurring lysine succinylation[1,2], are central to the regulation of chromatin-based processes. However, the mechanism and functional consequences of histone succinylation are unknown. Here we show that the α-ketoglutarate dehydrogenase (α-KGDH) complex is localized in the nucleus in human cell lines and binds to lysine acetyltransferase 2A (KAT2A, also known as GCN5) in the promoter regions of genes. We show that succinyl-coenzyme A (succinyl-CoA) binds to KAT2A. The crystal structure of the catalytic domain of KAT2A in complex with succinyl-CoA at 2.3 Å resolution shows that succinyl-CoA binds to a deep cleft of KAT2A with the succinyl moiety pointing towards the end of a flexible loop 3, which adopts different structural conformations in succinyl-CoA-bound and acetyl-CoA-bound forms. Site-directed mutagenesis indicates that tyrosine 645 in this loop has an important role in the selective binding of succinyl- CoA over acetyl-CoA. KAT2A acts as a succinyltransferase and succinylates histone H3 on lysine 79, with a maximum frequency around the transcription start sites of genes. Preventing the α-KGDH complex from entering the nucleus, or expression of KAT2A(Tyr645Ala), reduces gene expression and inhibits tumour cell proliferation and tumour growth. These findings reveal an important mechanism of histone modification and demonstrate that local generation of succinyl-CoA by the nuclear α-KGDH complex coupled with the succinyltransferase activity of KAT2A is instrumental in histone succinylation, tumour cell proliferation, and tumour development.

Metabolic enzymes such as pyruvate kinase M2, fumarase, and pyruvate dehydrogenase complex translocate into the nucleus and have instrumental roles in the epigenetic regulation of gene expression and DNA repair[3–5]. KAT2A, a member of the GCN5-related *N*-acetyltransferase (GNAT) superfamily, was identified as a histone acetyltransferase (HAT) that binds to acetyl-CoA and transfers its acetyl group to histones[6,7]. Mass spectrometric analyses of immunoprecipitated KAT2A from human HEK-293 cells and U251 glioblastoma (GBM) cells identified several known KAT2A-associated proteins, such as histone H3, RAD50, and TAF6L (Supplementary Table 1); it also revealed that oxoglutarate dehydrogenase (OGDH) (Extended Data Fig. 1a), which is a component of the α-KGDH complex that catalyses the conversion of α-ketoglutarate (α-KG) to succinyl- CoA, interacts with KAT2A. In addition, immunoblotting analyses of immunoprecipitated endogenous KAT2A with antibodies against the three components of α-KGDH—OGDH, dihydrolipoyl succinyltransferase (DLST), and dihydrolipoyl dehydrogenase (DLD)—revealed that these endogenous proteins were associated with each other (Fig. 1a). Cell fractionation (Fig. 1b, Extended Data Fig. 1b) and immunofluorescence (Extended Data Fig. 1c) analyses of U251 cells revealed that about 1–1.6% of total OGDH, DLST, and DLD was localized in the

nucleus (Extended Data Fig. 1b). About 13–16% of nuclear α-KGDH bound to KAT2A (Extended Data Fig. 1d, top), whereas about 2.3% of KAT2A (Extended Data Fig. 1d, bottom), which was found in nuclei but not in mitochondria (Extended Data Fig. 1e, f), interacted with OGDH.

To determine which component of the α-KGDH complex binds to KAT2A, we depleted individual components of α-KGDH in U251 cells (Fig. 1c, top) and incubated an immunoprecipitated α-KGDH complex depleted of different components with purified His–KAT2A. Immunoblotting analyses demonstrated that OGDH depletion, which did not affect the interaction between DLST and DLD (Extended Data Fig. 1g), abolished the interaction between KAT2A and the DLST–DLD complex (Fig. 1c, bottom). By contrast, depletion of DLST or DLD had no effect on the binding of OGDH to KAT2A (Fig. 1c, bottom). Co-immunoprecipitation analyses showed that OGDH depletion disrupted the association of endogenous KAT2A with the DLST–DLD complex in U251 cells (Extended Data Fig. 1g). These results suggest that OGDH binds to KAT2A.

We next used NLStradamus software[8] to analyse the amino acid sequences of OGDH, DLST, and DLD and found a putative nuclear localization sequence (NLS) in DLST. We mutated the Arg224 and Lys226 residues in the putative NLS into alanine and glutamic acid, respectively, and found that expression of the DLST(R224A/K226E) mutant reduced nuclear accumulation of the α-KGDH complex (immunofluorescence analyses, Extended Data Fig. 1h; cell fractionation, Fig. 1d and Extended Data Fig. 1i). These results indicate that Arg224 and Lys226 in the NLS of DLST are essential for nuclear translocation of the α-KGDH complex.

To understand the nuclear function of the α-KGDH complex, we investigated whether the nuclear α-KGDH complex, which generates succinyl-CoA, contributes to histone succinylation. As shown in Fig. 2a, expression of DLST(R224A/K226E), which did not alter α-KGDH activity (Extended Data Fig. 2a), total cellular levels of acetyl- CoA or succinyl-CoA (Extended Data Fig. 2b), or total cellular protein succinylation (Extended Data Fig. 2c), markedly reduced histone H3 succinylation in U251 cells. Given that KAT2A associated (Fig. 1a) and co-localized with α-KGDH and histone H3 (Extended Data Fig. 2d), we depleted KAT2A in U251 cells; this resulted in an approximately 35% reduction in histone H3 succinylation and substantial inhibition of histone H3 K9 and K14 acetylation (Fig. 2b). These results suggest that the nuclear α-KGDH complex and KAT2A are involved in histone H3 succinylation.

Because KAT2A binds to acetyl-CoA and acts as a histone acetyl transferase, we investigated whether KAT2A directly transfers the succinyl group of succinyl-CoA to histone H3. We performed an *in vitro* succinylation assay and showed that wild-type His–KAT2A, but not heat-inactivated His–KAT2A, succinylated histone H3 (Fig. 2c). Notably, KAT2A-mediated histone H3 succinylation was inhibited by CoA at high doses (Extended Data Fig. 2e). These results suggest that CoA competes with succinyl-CoA to bind to KAT2A and that the CoA group in succinyl-CoA is involved in its interaction with KAT2A.

To further understand KAT2A-mediated histone H3 succinylation, we crystallized the catalytic domain of KAT2A (residues 497–662) and its complex with succinyl-CoA. We obtained two crystal forms— P41212 and P213—for the apo and complex forms of KAT2A, respectively. The structures were analysed by molecular replacement with the known structure of the KAT2A–acetyl-CoA complex (Protein Data Bank ID: 1Z4R)[9,10]. To avoid model bias, we removed the acetyl-CoA moiety from the model for molecular replacement. We refined the final crystal structures to 2.9 Å resolution for the apo protein and 2.3 Å resolution for the complex (Extended Data Table 1). The overall structures of apo KAT2A and KAT2A–succinyl-CoA are similar to that of the KAT2A–acetyl-CoA complex, with root-mean-square deviations of 1.38 Å and 1.39 Å, respectively, for 163 common Cα atoms (Fig. 2d). Succinyl-CoA has a similar chemical structure to acetyl-CoA (Extended Data Fig. 2f) and uses its CoA moiety to bind to a deep hydrophobic pocket in KAT2A. Superimposition of the apo, succinyl-CoA-bound, and acetyl-CoA-bound structures of KAT2A demonstrated major differences in three loop regions (Fig. 2d). Notably, loop 2, which connects helices α 1 and α 2 (residues 530–535) was drawn closer to the binding pocket by about 2.2 Å upon binding of either acetyl-CoA or succinyl-CoA (Fig. 2d). Loop 3, which connects helix α 7 and strand β 7 (residues 639–648), can affect substrate specificity[11,12]. Compared with acetyl-CoA, succinyl-CoA makes additional Van der Waals interactions with side chains of M534, Y645, and A648 on KAT2A and forms hydrogen bonds with the side chain of Y645 and the main-chain carbonyl of Y613 (Extended Data Fig. 2g). In particular, the contacts made by the succinyl group with Y645 and A648 push loop 3 of KAT2A outward to a more distant location to accommodate the longer succinyl group (Fig. 2e). Loop 1, which connects helix α 1 and strand β 1 (residues 507–513), is distant from the active site of KAT2A (Fig. 2d). Because loop 1 is associated with high-temperature factors in all three structures, we consider this region inherently flexible. Therefore, structural variations in loop 1 do not necessarily correlate with substrate binding.

The contact between succinyl-CoA and loop 3 is closer than that between acetyl-CoA and loop 3 (Fig. 2e), suggesting that succinyl- CoA binds to KAT2A with a higher affinity than does acetyl-CoA. As expected, mixing purified KAT2A with purified histone H3 in the presence of equal amounts of succinyl-CoA and acetyl-CoA showed that succinyl-CoA markedly inhibited KAT2A-mediated H3K9 acetylation, whereas acetyl-CoA caused a much smaller decrease in KAT2A-mediated histone H3 succinylation (Extended Data Fig. 2h). In addition, we measured the velocity of enzyme-catalysed reaction at infinite concentration of substrate (V_{max}) and Michaelis constant (K_m) of the modification of histone H3 by KAT2A in the presence of succinyl-CoA or acetyl-CoA. The K_m of KAT2A was lower towards succinyl-CoA than that towards acetyl-CoA, suggesting that KAT2A has a higher binding affinity for succinyl-CoA than for acetyl-CoA (Extended Data Fig. 2i). In addition, KAT2A succinylated histone H3 with a 20% higher velocity than that with which it acetylated histone H3 (Extended Data Fig. 2j). Disruption of the interaction between succinyl- CoA and Y645 in KAT2A by mutating Y645 to alanine reduced the binding ability and catalytic activity of KAT2A towards succinyl-CoA but not towards acetyl-CoA (Extended Data Fig. 2i). Consistent with these *in vitro* results, reconstituted expression of the KAT2A(Y645A) mutant in U251 cells with depleted endogenous KAT2A, which did not affect histone H3 K14 acetylation, reduced histone H3 succinylation when compared with reconstituted

expression of wild-type KAT2A (Fig. 2f). These results indicate that Y645 in KAT2A binds specifically to succinyl-CoA and contributes to enhanced binding of KAT2A to succinyl-CoA.

By comparing the structure of the KAT2A–succinyl-coA complex to that of *Tetrahymena thermophila* KAT2A (ttKAT2A) in complex with a peptide-CoA bisubstrate[13], we found that the succinyl group partially occupies the binding site of the lysine substrate (Extended Data Fig. 2g). Similar stereochemical conflicts were also noted in the structures of KAT2A in complex with propionyl-CoA and butyryl-CoA[14]. We hypothesize that during catalysis, the acyl chain flips from the binding pocket (Fig. 2d, e) into an alternative pocket in the enzymatic active site to accommodate the binding of a lysine substrate and allow subsequent lysine succinylation. KAT2A has two such alternative pockets that could potentially accommodate succinyl or an even longer acyl chain; one is surrounded by ^{643}KDYEGA^{648} in loop 3, ^{575}EI^{576} in β 4, and ^{612}TY^{613} in β 5 (Extended Data Fig. 2k, magenta) whereas the other is surrounded by ^{531}LPR^{534} in loop 2 and ^{614}ADEYA^{618} in α 5 (Extended Data Fig. 2g, k, cyan). This situation is similar to that of EP300[15] (also known as p300), a HAT from the GNAT superfamily that catalyses the transfer of acetyl and small hydrophobic acyl groups to histone H3. Although EP300 can use a few acyl-CoA groups, its activity gets weaker with increasing acyl chain length[16], possibly owing to the size and hydrophobic nature of the flip pocket that excludes long-chain and charged acyl-CoA (for example, succinyl-CoA) variants. As expected, purified EP300 failed to catalyse H3 succinylation (Extended Data Fig. 2l).

We performed mass spectrometric analyses of KAT2A-succinylated histone H3 and found that H3K79 was succinylated (Extended Data Fig. 3a). H3K79 succinylation, which was also detected by a specific antibody (Extended Data Fig. 3b), was blocked by mutating K79 into arginine (Fig. 3a). Consistent with this finding, histone H3K79 succinylation was identified in U87 and U251 cells by immunoblotting (Fig. 3b) and mass spectrometric analyses (Extended Data Fig. 3c), and this succinylation was reduced by KAT2A depletion (Fig. 3b and Extended Data Fig. 3d), but not EP300 depletion (Extended Data Fig. 3e). However, quantification of succinyl-CoA and acetyl-CoA revealed that the nucleus contains much less succinyl-CoA than acetyl-CoA in both U87 and U251 cells (Extended Data Fig. 3f). Because KAT2A interacts with the α-KGDH complex in the nucleus, we hypothesized that succinyl-CoA generated by this complex serves as a local source of succinyl-CoA for KAT2A-dependent histone succinylation. To test this hypothesis, we performed an *in vitro* succinylation assay by mixing purified KAT2A, histone H3, NAD^+, α-KG and CoA in the presence of immunoprecipitated wild-type OGDH or inactive OGDH(P459A/Y460A), which has lost its enzymatic activity (Extended Data Fig. 3g). We showed that only KAT2A coupled with wild-type OGDH succinylated H3K79 (Fig. 3c), and this succinylation was observed even in the presence of a high concentration of acetyl-CoA (Extended Data Fig. 3h). In addition, immunoprecipitated KAT2A from the nuclei of 293 cells expressing wild-type DLST but not DLST(R224A/K226E) succinylated purified histone H3 in the presence of α-KG and absence of exogenous succinyl-CoA (Extended Data Fig. 3i). Consistent with this finding, reconstituted expression of the DLST(R224A/K226E) mutant reduced H3K79 succinylation by about 70%, but did not reduce H3K9 or H3K14 acetylation (Fig. 3d). These

results indicate that nuclear α-KGDH couples with KAT2A to mediate H3K79 succinylation.

KAT2A in the SPT–ADA–KAT2A–acetyltransferase (SAGA) complex functions as a HAT, and disruption of this complex inhibits histone acetylation[6]. Depletion of TAF9 RNA polymerase II, which is a core component of the human SAGA complex that is required for its function[6], reduced acetylation of histone H3K9 and H3K14 without affecting succinylation of H3K79 (Extended Data Fig. 3j). Thus, in different complexes, KAT2A functions as either a HAT or a succinyltransferase.

To assess the chromatin occupancy of H3K79 succinylation and its correlation with KAT2A at a high resolution, we performed chromatin immunoprecipitation–sequencing (ChIP–seq) assays. We identified 17,107 H3K79 succinylation-enriched peaks, 12,505 KAT2A-binding-enriched peaks, and 249 α-KGDH-binding-enriched peaks, which were widely distributed in the genome of U251 cells. Compared with the non-repetitive genome background, the ChIP–seq peaks for H3K79 succinylation (50.6%), KAT2A-binding (26.8%), and α-KGDH-binding (84.3%) were enriched in the gene promoter regions (Extended Data Fig. 3k), and the average distributions of H3K79 succinylation, KAT2A, and α-KGDH in the promoter regions were strongly enriched at transcription starting sites (TSSs) and adjacent regions within 2 kb (Fig. 3e). We identified 7,186 H3K79-succinylated (Supplementary Table 2), 1,868 KAT2A-binding (Supplementary Data Table 3), and 228 α-KGDH-binding (Supplementary Table 4) gene promoters (Extended Data Fig. 3l). Furthermore, 676 annotated gene promoter regions were occupied by both H3K79 succinylation and KAT2A (Supplementary Table 5); these regions represented 9.4% of H3K79 succinylation peaks and 36.2% of KAT2A-occupying peaks, suggesting that the binding of KAT2A to gene promoter regions for succinylation is transient and dynamic and that ChIP–seq analyses identify KAT2A-associated gene promoters only at the point when KAT2A binds to histone H3 (a similar situation also applies for α-KGDH). By contrast, H3K79 succinylation is relatively stable and can be accumulated. This assumption was supported by results showing that the purified KAT2A that was pulled down by immobilized and biotin-labelled nucleosome was dissociated from the immobilized nucleosome and succinylated K79 of histone H3 from purified and soluble nucleosomes (Extended Data Fig. 3m). A high percentage of α-KGDH-binding peaks (198 of 228, 86.8%) overlapped with peaks of H3K79 succinylation (Supplementary Table 6), suggesting that α-KGDH has a critical role in H3K79 succinylation. In addition, 59 (25.9%) of the α-KGDH-bounded-promoters were co-occupied by KAT2A (Supplementary Table 7), suggesting that α-KGDH and KAT2A dissociate from histone with differing dynamics. To further support the idea that KAT2A is instrumental in H3K79 succinylation, we showed that KAT2A depletion resulted in a 96% decrease in H3K79 succinylation-enriched gene promoters (Extended Data Fig. 3n, Supplementary Table 8).

We next used gene set enrichment analysis (GSEA) to examine genes with H3K79 succinylation in their promoter regions for 1,329 canonical pathways defined from various databases. H3K79- succinylated genes were significantly enriched in 130 of 1,329 cell signalling pathways ($P < 0.001$, FDR $q < 0.001$) (Extended Data Fig. 4). Hypergeometric tests on RNA sequencing (RNA-seq) data revealed that important cell signalling pathways,

such as the phosphoinositide 3-kinase (PI3K), activator protein 1 (AP1), and cell cycle pathways, were significantly suppressed by the expression of V5-tagged shRNA- resistant rDLST(R224A/K226E) (V5–rDLST(R224A/ K226E)) or Flag–rKAT2A(Y645A) mutants ($P < 0.01$, FDR $q < 0.05$) (Extended Data Fig. 5a–c). In addition, *PIK3R1* (encoding PI3K regulatory subunit alpha, also known as p85α), *JUN* (encoding c-Jun), and *PRKDC* (encoding DNA-dependent protein kinase, catalytic subunit, also known as DNA-PKcs) were among those genes with the most significantly changed expression, the most important regulators in the significantly enriched pathways ($P < 0.01$, FDR $q < 0.05$), or important hitches (critical genes involved in the function of multiple signalling pathways) between these pathways. KAT2A depletion significantly reduced succinylation in these selected gene promoter regions ($P < 0.01$) (Fig. 3f). Consistently, the mRNA (Extended Data Fig. 5d and 5e) and protein (Fig. 3g and 3h) expression of these genes in U87 cells was inhibited by reconstituted expression of Flag– rKAT2A(Y645A) or V5–rDLST(R224A/K226E). Similar inhibition was also observed in U251 cells (Extended Data Fig. 5f–i). Together, these results strongly suggest that the α-KGDH complex, associated with KAT2A in gene promoter regions, plays an instrumental role in the regulation of gene expression.

H3K79 succinylation occurred in 7,186 genes, and is therefore likely to affect many cellular activities and cell growth. Reconstituted expression of Flag–rKAT2A(Y645A) and V5–rDLST(R224A/K226E) inhibited proliferation of both U87 (Fig. 4a) and U251 (Extended Data Fig. 6a) cells. We then intracranially injected U87 cells with reconstituted expression of wild-type Flag–rKAT2A, Flag–rKAT2A(Y645A), wild-type V5–rDLST, or V5–rDLST(R224A/K226E) into athymic nude mice. Expression of the mutant proteins inhibited brain tumour growth (Fig. 4b and Extended Data Fig. 6b) and reduced expression of Ki67 (Fig. 4c and Extended Data Fig. 6c), p85α, DNA-PKcs, and c-Jun (Extended Data Fig. 6d) in tumour cells. Immunoblotting analyses of histone extracts from tumours expressing these mutants revealed a reduction in histone H3K79 succinylation but not in H3K9 or H3K14 acetylation (Fig. 4d, Extended Data Fig. 6e, f). These results support the importance of the nucleus-localized α-KGDH complex in brain tumour growth.

Histone modifications play critical roles in the regulation of gene expression[6]. We have shown that the α-KGDH complex interacts with KAT2A in the nucleus. This enables KAT2A to access the concentrated succinyl-CoA generated locally by the α-KGDH complex and thereby compensates for the low concentration of succinyl-CoA in the nucleus. Structural analyses demonstrated that the succinyl group of succinyl-CoA protrudes to the very end of a flexible loop 3 to interact specifically with Y645 in loop 3, leading to increased binding of succinyl-CoA (over acetyl-CoA) to KAT2A. The high binding affinity of succinyl-CoA and high local concentrations of succinyl-CoA generated by the KAT2A-associated α-KGDH complex facilitated histone succinylation in spite of the relatively low concentration of succinyl- CoA in the nucleus. Thus, KAT2A, as well as being a HAT, is also a histone succinyltransferase; these findings underscore the importance of the coupling of the metabolic enzyme complex α-KGDH and KAT2A for gene expression, tumour cell proliferation, and tumour formation.

METHODS

No statistical methods were used to predetermine sample size. The experiments were not randomized and the investigators were not blinded to allocation during experiments and outcome assessment, unless otherwise stated.

Materials

The antibodies used in the experiments are listed in Supplementary Table 9. DNase-free RNase A and propidium iodide were purchased from EMD Biosciences. PolyJet *in vitro* DNA transfection reagent was purchased from SignaGen Laboratories. Purified active full-length KAT2A was obtained from Cayman Chemicals. Bacterial purified human histone H3 protein was obtained from New England BioLabs. GelCode Blue Stain Reagent was obtained from Pierce. H3K79 (EIAQDFKTDLRFQ) and succinylated H3K79 (EIAQDFK[succinylated] TDLRFQ) peptides were obtained from Signallway Antibody. The *in vitro* assembled nucleosome containing biotin-labelled DNA was obtained from EpiCypher. The *in vitro* assembled nucleosome with His-histone H3 was obtained from BPS Bioscience.

Cell lines and cell culture conditions

Parental U87, U251, and 293 cells were obtained from the American Type Culture Collection. Parental U87 and U251 cell lines used in the experiments were authenticated by using short tandem repeat profiling. The cells were examined for mycoplasma contamination by using a Cycleave polymerase chain reaction (PCR) mycoplasma detection kit (Takara Bio). U87 and U251 GBM cells and 293 cells were maintained in Dulbecco's modified Eagle's medium supplemented with 10% bovine calf serum (HyClone). Protein expression and reconstitution experiments were conducted using established stable cell lines.

DNA constructs and mutagenesis

PCR-amplified human *OGDH*, *DLST*, and *DLD* were cloned into pcDNA6V5HisB and pcDNA3.1/hygro(+)-Flag vectors. A full-length *KAT2A* open reading frame was cloned into pcDNA3.1/hygro(+)- Flag, pcDNA6V5HisB, and pET32a vectors. A full-length *H3F3A* (encoding histone H3.3) open reading frame was cloned into the pET32a vector. The pET28a-LIC–KAT2A core domain (encoding residues 47–210) was obtained from Addgene (plasmid #25482). pcDNA6V5HisB–DLST(R224A/K226E), pcDNA3.1/ hygro(+)-Flag–KAT2A(Y645A), and pET32a–H3(K79R) were made by using a QuikChange site-directed mutagenesis kit (Stratagene).

A control pGIPZ vector was generated by using the control oligonucleotide GCTTCTAACACCGGAGGTCTT. pGIPZ *KAT2A* shRNA was generated with GCATTAAAGCAGCGTATC. pGIPZ *OGDH* shRNA was generated with CATCTACCACTTGCAATTA. A control pLKO-1 vector was generated with the control oligonucleotide CCGCAGGTATGCACGCGT. pLKO-1 *OGDH* (TRCN0000028580), *DLST* (TRCN0000344818), *DLD* (TRCN0000275684), and *TAF9* (TRCN0000014568) shRNAs were obtained from Sigma-Aldrich.

Mass spectrometric analysis

To identify KAT2A-dependent succinylation of lysines on histone H3, an *in vitro* KAT2A-succinylated sample of purified histone H3 was exhaustively acetylated with acetic anhydride and triethylamine in acetonitrile, evaporated to dryness, and resuspended in 50 mM ammonium bicarbonate buffer containing RapiGest (Waters Corporation). The sample was heated to 95 °C for 10 min and then allowed to cool; 100 ng of sequencing-grade modified trypsin (Promega) was then added to the sample. Digestion of the sample took place overnight at 37 °C and was analysed using LC–MS/MS with an Orbitrap Elite mass spectrometer (Thermo Fisher Scientific). Proteins were identified via a database search of the fragment spectra against the national Swiss-Prot protein database (European Bioinformatics Institute) by using the Mascot software program (version 2.3; Matrix Science) and the SEQUEST software program (version 1.20) via Proteome Discoverer (version 1.3; Thermo Fisher Scientific). Specific succinylated H3 lysine identification was conducted as described previously[2].

To identify the KAT2A-interacting proteins, KAT2A and its interacting proteins were immunoprecipitated from U251 cells. The protein sample was heated to 95 °C in the presence of SDS–PAGE loading buffer for 10 min and then allowed to cool. The heated sample was loaded into and accumulated in an SDS–PAGE stacking gel via electrophoresis at 100 V for 5 min. Gel band samples were subjected to in-gel digestion, as described previously[3], and then analysed using LC–MS/MS with an Orbitrap Fusion Tribrid mass spectrometer (Thermo Fisher Scientific) interfaced with a Dionex UltiMate 3000 Binary RSLCnano System. The raw data files were processed using the Proteome Discoverer software program (version 1.4), and the International Protein Index database was searched for spectra by using the Mascot software program (version 2.3.02) on an in-house server. Search results were trimmed to a 1% false discovery rate using the Percolator algorithm (Matrix Science).

Transfection

Cells (4×10^5) were cultured in a 60-mm dish for 18 h and then transfected using PolyJet *in vitro* DNA transfection reagent (SignaGen Laboratories) according to the manufacturer's instructions.

Nuclear fractionation analysis

Nuclei from U87 or U251 cells were obtained using a Nuclei Pure Prep Nuclei Isolation Kit from Sigma-Aldrich according to the manufacturer's guidelines.

Histone extraction

Cells were collected and washed twice with ice-cold PBS, then resuspended in triton extraction buffer (TEB: PBS containing 0.5% Triton X-100 (v/v), 2 mM phenylmethylsulfonyl fluoride (PMSF), 0.02% (w/v) NaN_3) at a cell density of 10^7 cells per ml. Cells were then lysed on ice for 10 min with gentle stirring and centrifuged at 2,000 r.p.m. for 10 min at 4 °C. The supernatant was removed and discarded. The cells were washed with TEB and centrifuged as before, and then the pellet was resuspended in 0.2 N HCl at a cell density of 4×10^7cells per ml. Histones were acid extracted overnight at 4 °C.

Then, samples were centrifuged at 2,000 r.p.m. for 10 min at 4 °C. The supernatant was removed and protein content determined using the Bradford assay, and pH was neutralized by adding 10% (v/v) 2 M $NaHCO_3$. Aliquots were stored at − 20 °C.

Immunofluorescent microscopic analysis

Cells were seeded on coverslips 24 h before fixation for immunofluorescent assays. The cells were washed three times in PBS (5 min per wash) and then fixed and permeabilized in a freshly prepared mixture of methanol and acetone (80:20) for 10 min at − 20 °C. The cells were then washed three times in cold PBS as before. Cells were blocked for 1 h in a blocking solution (3% bovine serum albumin and 1% horse serum) at 25 °C. Primary antibodies diluted at 1:100 in a blocking solution were added and the mixture was incubated overnight at 4 °C. The cells were again washed three times in PBS. Secondary antibodies diluted at 1:2,000 in a blocking solution were added and the mixture incubated for 1 h at room temperature. Once more, the cells were washed three times in PBS. ProLong Gold antifade reagent with DAPI medium was added. The slides containing the cells were allowed to sit for 10 min in the dark. The coverslips were sealed with a nail hardener. Immunofluorescent microscopic images of the cells were obtained and viewed with an IX81 confocal microscope system (Olympus America).

Cell proliferation assay

A total of 5×10^4 cells were plated and counted 9 days after seeding in Dulbecco's modified Eagle's medium with 10% bovine calf serum. Data are presented as the means ± s.d. from three independent experiments.

Immunoprecipitation and immunoblotting analysis

Proteins were extracted from cultured cells using a modified buffer, and immunoprecipitation and immunoblotting analyses with corresponding antibodies were performed as described previously[3]. A lysis buffer with 0.2% Triton X-100 was used for immunoprecipitation of Flag-rKAT2A expressed in HEK-293 cells. The peptide of H3K79 (EIAQDFKTDLRFQ) was added in the antibody to histone H3K79 succinylation (5 μg ml^{-1}) to further enhance the specificity. The intensities of immunoblotting analyses were measured using ImageJ software.

Expression and purification of recombinant proteins

Full-length His–KAT2A and the His–KAT2A catalytic domain were expressed in BL21 strain of *Escherichia coli*. The cultures grew at 37 °C to an optical density (at a wavelength of 600 nm) of about 0.6 and were then treated with 0.5 mM isopropyl β-d-1-thiogalactopyranoside (IPTG) at 18 °C. Cell pellets were collected, resuspended in BugBuster lysis buffer (EMD Millipore) with a supplement of cocktail proteinase inhibitors and DNase I, and processed using sonication. Soluble His-tagged proteins were purified by using the ÄKTA system with 5 ml of a HisTrap column (GE Healthcare Life Sciences), as described previously[9]. The protein purity was identified via gel staining with GelCode Blue Staining.

Crystallization and structure determination

The purified recombinant KAT2A catalytic domain was dialysed with 20 mM HEPES-NaOH (pH 7.5) and 150 mM NaCl and concentrated to 4 mg ml^{-1} for crystallization. For co-crystallization, 10 mM succinyl-CoA was added to the protein solution. Prism-shaped crystals appeared within 1 day in hanging drops containing 1.5 μl protein solution and 0.5 μl mother liquor (in 0.1 M sodium acetate, pH 4.6, and 1.4 M ammonium sulphate or 0.5 M lithium chloride and 1.2 M ammonium sulphate). Crystals usually grew to full size within 7 days. KAT2A crystals were frozen in mother liquor substituted with 25% glycerol. X-ray diffraction data on the crystals were collected at 77 K by the Life Sciences Collaborative Access Team at the Advanced Photon Source. Data for the apo structure were collected at a wavelength of 0.97872 Å at Beamline 21-ID-F; data for the succinyl-CoA complex were collected at a wavelength of 0.97857 Å at Beamline 21-ID-G. One crystal was used for each structure, and values in parentheses (Extended Data Table 1) are for highest-resolution shell. Diffraction images were processed using HKL-2000 software. For structure determination, the human KAT2A–acetyl-CoA complex structure (Research Collaboratory for Structural Bioinformatics (RCSB) Protein Data Bank ID: 1Z4R) was used for molecular replacement. The acetyl-CoA ligand was removed from the model to reduce model bias. Molecular replacement was calculated using the Phaser software program in the PHENIX software suite[17]. The structure models were then manually adjusted using the Coot software program[18] and refined using PHENIX. The final coordinates of apo KAT2A have a MolProbity overall score of 1.80 and a clash score of 12.23, with 96.79% favoured, 3.21% allowed and no outlier in the Ramachandran plot, 0.32% rotamer outlier and no Cβ deviation. The final coordinates of succinyl- CoA complex have a MolProbity overall score of 1.40 and a clash score of 7.08, with 98.64% favoured, 1.36% allowed and no outlier in the Ramachandran plot, no rotamer outlier or Cβ deviation. Structure figures were prepared using the PyMOL molecular graphics system (version 1.2r3pre). The coordinates have been deposited at the RCSB Protein Data Bank under accession numbers 5TRM and 5TRL for the apo and succinyl-CoA structures, respectively.

In vitro α-KGDH enzymatic activity assay

Immunoprecipitated Flag-tagged α-KGDH from 293 cells was incubated with the α-KGDH buffer (50 mM MOPS HCl, pH 7.4, 0.2 mM $MgCl_2$, 0.01 mM $CaCl_2$, 0.3 mM cocarboxylase, 0.12 mM CoA, 2 mM β-nicotinamide adenine dinucleotide, 2.6 mM l-cysteine) and 5 mM α-ketoglutarate at 30 °C for 30 min. At the end of the reaction, 10 U diaphorase and 20 μM resazurin were added to generate a fluorescent signal in proportion to the amount of NADH generated by α-KGDH. The α-KGDH enzyme activity was measured via direct coupling of the NADH production with conversion of resazurin to resorufin by diaphorase. Resorufin was measured fluorometrically at an excitation wavelength of 544 nm and emission wavelength of 590 nm. Data are presented as the means ± s.d. of three independent experiments.

In vitro histone H3 succinylation assay

To analyse KAT2A-catalysed histone H3 succinylation, we incubated purified wild-type His–histone H3 or His–histone H3(K79R) with purified full-length active KAT2A in the

presence of HAT buffer (50 mM Tris-HCl, pH 8.0, 50 mM KCl, 5% glycerol, 0.1 mM EDTA, 1 mM dithiothreitol, 1 mM PMSF, 10 mM sodium butyrate) and 2 μM succinyl-CoA at 37 °C for 10 min. Histone H3 succinylation was determined by using immunoblotting analysis.

To analyse α-KGDH-dependent histone H3 succinylation, we incubated the immunoprecipitated Flag-tagged OGDH from 293 cells with purified wild-type histone H3, full-length active KAT2A, and 5 mM α-ketoglutaric acid in the presence of α-KGDH buffer (50 mM MOPS HCl, pH 7.4, 0.2 mM $MgCl_2$, 0.01 mM $CaCl_2$, 0.3 mM cocarboxylase, 0.12 mM CoA, 2 mM β-nicotinamide adenine dinucleotide, 2.6 mM l-cysteine) at 30 °C for 30 min. Histone H3 succinylation was determined with use of immunoblotting analysis.

To analyse nuclear α-KGDH–KAT2A complex-dependent histone H3 succinylation, we transfected the vector expressing wild-type Flag–rKAT2A with the vector expressing wild-type V5–rDLST or the V5–rDLST NLS mutant. The nuclear α-KGDH–KAT2A complex was immunoprecipitated with anti-Flag agarose beads. Purified wild-type histone H3, nuclear α-KGDH–KAT2A complex, and 5 mM α-ketoglutaric acid were incubated in the presence of α-KGDH buffer at 30 °C for 3 h. Histone H3 succinylation was determined by using immunoblotting analysis.

Steady-state kinetics of KAT2A activity for histone H3 modifications

Immunoprecipitated full-length Flag–KAT2A from 293 cells was immobilized on anti-Flag-agarose beads and incubated with purified histone H3 (4 μM) in HAT buffer in the presence of 0.009 μM, 0.027 μM, 0.082 μM, 0.247 μM, 0.741 μM, 2.222 μM, 6.667 μM, or 20.000 μM of acetyl-CoA or succinyl-CoA at 25 °C for 5 min. The reaction mixture was precipitated via centrifugation at 1,000*g* for 5 min. The production of CoA in the supernatant was quantitatively analysed using a modified protocol from the PicoProbe Acetyl-CoA Fluorometric Assay Kit (BioVision). In brief, 25 μl supernatant was mixed with 1 μl PicoProbe, 1 μl acetyl-CoA substrate mix, 2.5 μl acetyl-CoA enzyme mix, and 20.5 μl acetyl-CoA assay buffer. The CoA can react to form NADH, which interacts with OicoProbe to generate fluorescence (E_x/E_m = 535/587 nm). An identical reaction was set up for each acetyl-CoA or succinyl-CoA titration without KAT2A protein and used as the blank control. Data are presented as the means ± s.d. of three independent experiments.

Quantitative analysis of nuclear succinyl-CoA and acetyl-CoA

The nuclei were obtained from U251 and U87 cells and analysed using LC–MS/MS. In brief, nuclear extracts were processed for protein precipitation followed by solid-phase extraction. Fifteen per cent trichloroacetic acid (TCA) in water was applied to remove proteins and other interference substances from the nuclear samples. The supernatant was subsequently transferred to a Waters HLB solid-phase extraction cartridge for further sample clean-up. The final reconstitution samples were injected into a Gemini C6-phenyl 100 × 4.6 mm 3 μM high-performance liquid chromatography column (Phenomenex). The mobile phase consisted of ammonium acetate and acetic acid in both aqueous and organic phases. Data acquisition was performed using a 6460 Series Triple Quadrupole LC/MS (Agilent Technologies) via multiple reaction mode (MRM) electrospray positive mode.

Quantitative real-time PCR

Total RNA of cells was extracted using an RNeasy Plus Kit (QIAGEN). cDNA was prepared using a High Capacity cDNA Reverse Transcription Kit (Applied Biosystems). Quantitative real-time PCR analysis was performed by using 2 × iQ SYBR Green Supermix (Bio-Rad) in the following conditions: 5 min at 95 °C, and then 40 cycles at 95 °C for 30 s, 58 °C for 20 s, and 72 °C for 15 s using a Bio-Rad CFX96 Real-Time System. Data were normalized according to expression of a control gene (*ACTB*) in each experiment. The data are presented as the means ± s.d. from three independent experiments.

The following primer pairs were used for quantitative real-time PCR: *PIK3R1*, 5′-GGGTGAAGCTCGTGTGTGGA-3′ (forward) and 5′-GTGTGACCGAAGAC AGGGCT-3′ (reverse); *JUN*, 5′-TCTGGGAAGTGAGTTCGCCT-3′ (forward) and 5′-ATGCCTCCCGCACTCTTACT-3′ (reverse); *PRKDC*, 5′-AGGCGGCT TACCTGAGTGAT-3′ (forward) and 5′-CACGAAGGCCCGCTTTAAGA-3′ (reverse); and *ACTB*, 5′-CATCGAGCACGGCATCGTCA-3′ (forward) and 5′-TAGCACAGCCTGGATAGCAAC-3′ (reverse).

ChIP and ChIP–seq assay

ChIP was performed using a SimpleChIP Enzymatic Chromatin IP Kit (Cell Signaling Technology). Chromatin prepared from cells in a 15-cm dish was used to determine total DNA input and was incubated overnight with specific antibodies or normal rabbit IgG. The following primer pairs were used for candidate gene promoter region validation: *PIK3R1*, 5′ - CCGGCGTCCTGTGAG ATCC -3′ (forward) and 5′-GCAACTCCGGGGGCAAATG-3′ (reverse); *JUN*, 5′-AGTTCAACAACCGGTGCGAG-3′ (forward) and 5′-AGAGTCCCGGA GCCAACTTT-3′ (reverse); and *PRKDC*, 5′-GGAGCCGGTGTGCGTTG-3′ (forward) and 5′-GGCCGCGGATCAGTTGATGA-3′ (reverse).

ChIP sequencing was performed at the Sequencing and Microarray Facility at The University of Texas MD Anderson Cancer Center. In brief, indexed libraries were prepared from 20 ng Bioruptor-sheared (Diagenode) ChIP DNA using a Hyper Library Preparation Kit (Kapa Biosystems). The libraries were amplified using three cycles of PCR and then assessed for quality using a Fragment Analyzer High Sensitivity NGS Fragment Analysis Kit (Advanced Analytical Technologies) and quantified using a Qubit dsDNA HS Assay Kit (Thermo Fisher Scientific). The indexed libraries were pooled at three libraries per pool and sequenced in one lane of a HiSeq2000 Sequencer (Illumina) using the 36-nt single-read configuration.

RNA-seq

Total RNA was extracted from cells using a PureLinkTM RNA Mini Kit (Thermo Fisher Scientific). Illumina compatible libraries were prepared using the KAPA Stranded mRNA-Seq Library Preparation Kit for Illumina platforms (KAPA Biosystems). In brief, 250 ng total RNA was enriched for poly-A-tailed mRNA using Kapa's mRNA Capture beads. Poly-A-enriched RNA was fragmented to a median size of 150 bp using chemical fragmentation and converted into double- stranded cDNA with dUTP incorporated into the second cDNA

strand. The ends of the double-stranded cDNA were polished, 5′-phosphorylated, and 3′-A-tailed for the ligation of indexed adaptors. Adaptor-ligated DNA fragments were amplified by eight cycles of PCR. The strand with incorporated dUTP was not amplified. The resulting libraries were quantified by qPCR and assessed for size distribution using the 4200 TapeStation (Agilent Technologies), and then multiplexed (four per pool) and sequenced on the Illumina's NextSeq500 using the mid-output, 75-bp paired-end read format.

Analyses of RNA-seq and ChIP–seq data

We used a series of cutoffs to analyse the RNA-seq and ChIP–seq data and selected the genes that met the following two criteria: 1) expression that was significantly altered by either KAT2A(Y645A) or DLST(R224A/K226E) mutant expression ($P < 0.05$ and FDR $q < 0.1$ in the RNA-seq data); and 2) enriched H3K79 succinylation in promoter regions (fold enrichment > 2 and FDR $q < 0.1$ in the ChIP–seq data).

Gene set enrichment and pathway analyses

GSEA of the results from next-generation sequencing data was performed using GSEA v2.2.3 software with the gene lists for 1,329 canonical pathways in collection C2.CP from Molecular Signature Database (MSigDB) V5.2. Both the GSEA software and the MSigDB are maintained by the Broad Institute. Collection C2.CP includes curated pathway maps from multiple established pathway databases, including REACTOME, KEGG, BIOCARTA, PANTHER and Pathway Interaction Database (PID).

GSEA of the ChIP–seq data was based on the fold-enrichment (FE) measurement for 20,338 genes by using the 'GSEA preranked' option.

GSEA results were visualized using the EnrichmentMap v2.0.1 plugin in the Cytoscape v3.2.1 network visualization platforms.

Hypergeometric tests were used to identify pathways enriched with significantly altered genes. We used the ConsensusPathDB-human (CPDB) platform developed at the Max Planck Institute for Molecular Genetics, which contains 5,068 canonical pathways defined in 12 public sources (including KEGG, REACTOME, BIOCARTA, PID, WikiPathways, and NetPath).

$$P(X=k)=\frac{\binom{K}{k}\binom{N-K}{n-k}}{\binom{N}{n}}$$

The hypergeometric distribution measured the statistical significance of a certain number (k) of pathways grouped from the genes with significant expression changes (n, the number of genes that meet the criteria of $P < 0.05$ and $q < 0.1$ for RNA-seq; fold enrichment > 2 and $q < 0.1$ for ChIP–seq). N represents the total number of genes identified in both the ChIP–seq and RNA-seq analyses. K represents the number of member genes identified in both the RNA-seq and ChIP–seq analyses, and k represents the number of genes from each K that passed the significance cutoff ($P < 0.05$ and $q < 0.1$ for RNA-seq; fold enrichment > 2 and $q < 0.1$ for ChIP–seq). We calculated the P value $P(X \geq$

k) as the probability of randomly drawing *k* or more genes from the gene population (*n*) that passed the cutoff for significant changes in expression. We selected pathways with $P < 0.01$ and FDR $q < 0.05$ to be candidates for follow-up studies. We performed visualization revealing the relationship of the selected genes with 10 critical pathways using the EnrichmentMap v2.0.1 plug-in in the Cytoscape v3.2.1 network visualization platform.

Intracranial injection

U87 cells (5×10^5) with or without modified gene expression were intracranially injected into female 4-week-old athymic nude mice (in 5 μl of Dulbecco's modified Eagle's medium per mouse), as described[3]. Five mice were randomly grouped before tumour cell injection. The mice were killed 30 days after injection. The brains were removed, fixed in 4% formaldehyde, and embedded in paraffin. Tumour formation was determined by haematoxylin and eosin staining. Tumour volume was calculated by $0.5 \times L^2 \times W$.

Mice were monitored for signs of tumour burden, including weight loss, laboured breathing, hunched posture, and abnormal vocalization when handled. If mice exhibited any indication of these signs, they were killed together with other experimental mice. Otherwise, all mice were killed 30 days after injection. The use of animals was approved by the Institutional Review Board of The University of Texas MD Anderson Cancer Center.

Immunohistochemical analysis

Mouse tumour samples were fixed, paraffin-embedded, sectioned (5 μm), and stained with Mayer's haematoxylin and eosin (BioGenex Laboratories). Slides were then mounted using universal mount (Research Genetics) and examined with a light microscope.

Sections of paraffin-embedded xenograft tissue were stained with antibodies against telomerase or Ki67 or with nonspecific IgG as a negative control. The immunohistochemical staining was performed using a VECTASTAIN ABC kit (Vector Laboratories) according to the manufacturer's instructions.

Statistical analysis

The significance of differences in the experimental data was determined using Student's *t*-test (two-tailed) unless specifically indicated. Differences in means were considered statistically significant at $P < 0.05$. The *P* and FDR *q* values in the GSEA were obtained from 1,000 permutations[19].

Data availability

The data that support the findings of this study are available from the corresponding author on request. The ChIP–seq and RNA-seq data have been deposited in the Gene Expression Omnibus (GEO) with the accession numbers GSE97994 (ChIP–seq data) and GSE98050 (RNA-seq data). The crystal structural coordinates were deposited at the RCSB Protein Data Bank (PDB ID 5TRM and 5TRL for the apo and succinyl-CoA structures, respectively).

Extended Data

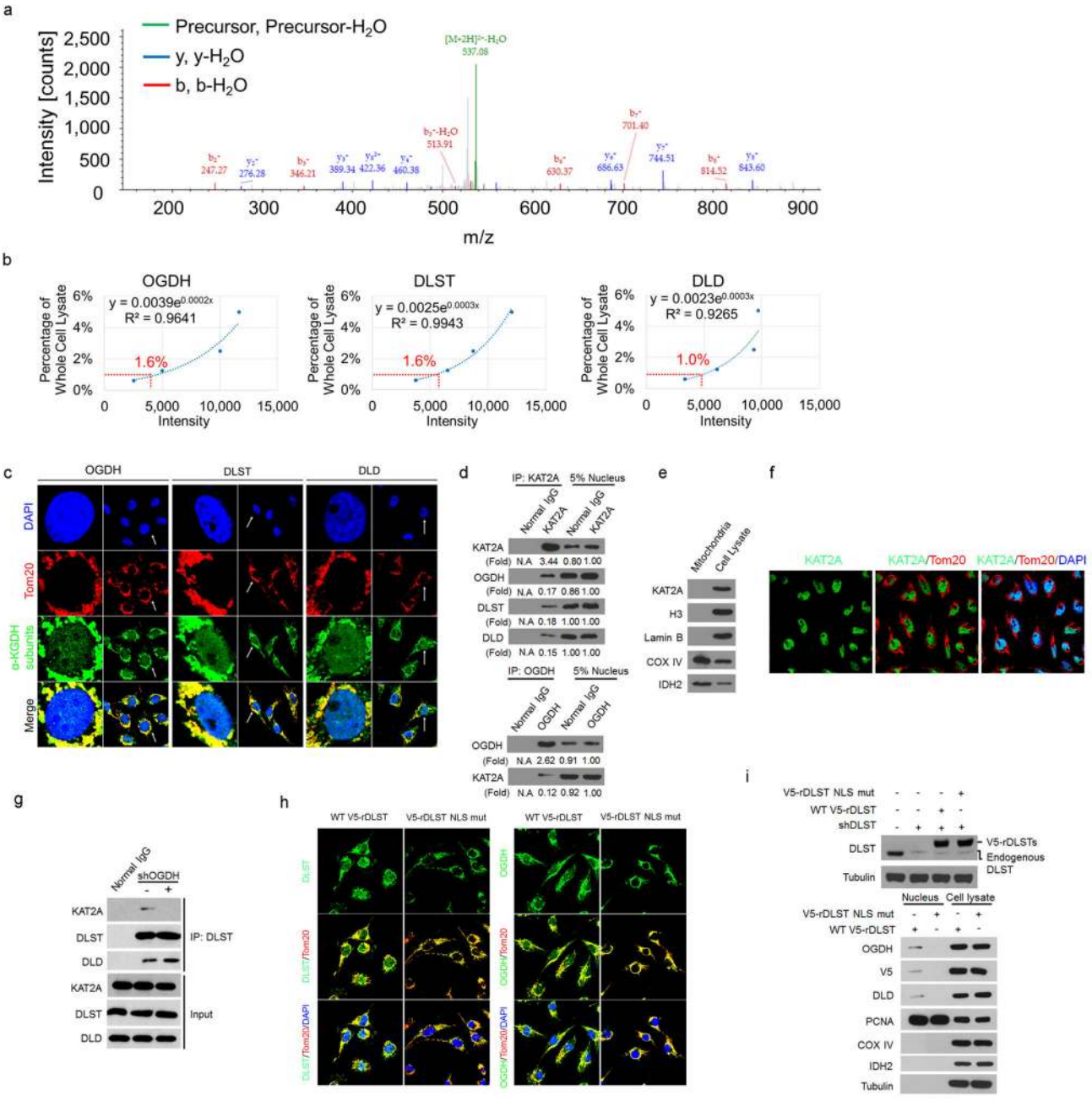

Extended Data Figure 1. KAT2A interacts with the α-KGDH complex in the nucleus

a, OGDH binds to KAT2A. KAT2A was immunoprecipitated from U251 cells using an anti-KAT2A antibody. The immunoprecipitate was analysed by mass spectrometry. A specific peptide (920-DMVGQVAIT-929) of OGDH was identified. The IonScore is 30, the *q* value is 0.004, and the Exp value (*P*) is 0.1792. One-sided *t*-tests were conducted. Representative results of two experiments are shown. **b**, Quantitative analyses of α-KGDH subunits in the nucleus. Immunoblotting analyses of α-KGDH subunits in the nucleus extraction of U251

cells were performed with the indicated antibodies displayed in Fig. 1b. The quantitative standard curves were used to determine the percentage of nuclear OGDH, DLST, and DLD. The *x*-axis presents the intensities of quantified proteins detected by immunoblotting analysis, and the *y*-axis presents the percentage of whole-cell lysate corresponding to each quantified protein. The percentages of nuclear OGDH, DLST, and DLD were calculated using the equations displayed above the standard curves. Representative images of triplicate experiments are shown. The R^2 values represent the relationship between log Y and X to the linear model ($\log Y = \log[A + B] \times X$). Y, percentage of whole cell lysate; X, intensity. **c**, Nuclear distribution of the α-KGDH complex. Immunofluorescent staining of U251 cells was performed with anti-OGDH, anti-DLST, or anti-DLD antibodies (green). The mitochondria and nuclei were stained with an anti-Tom20 antibody (red) and DAPI (blue), respectively. Representative images of more than 50 cells are shown. The majority of the α-KGDH complex overlapped with the mitochondrial protein Tom20, indicating primary mitochondrial localization of the α-KGDH complex. **d**, Quantitative analyses of the interaction between KAT2A and α-KGDH subunits. Immunoprecipitation analyses of U251 cell nuclei with anti-KAT2A or anti-OGDH antibodies were performed. KAT2A-or OGDH-associated proteins were analysed via immunoblotting analyses. Representative images of triplicate experiments are shown. **e**, **f**, KAT2A is not localized in mitochondria. **e**, Immunoblotting analyses of the mitochondria extraction and total cell lysate of U251 cells were performed with the indicated antibodies. Representative images of triplicate experiments are shown. **f**, Immunofluorescent analyses of U251 cells were performed with DAPI (blue) and anti-KAT2A (green) and anti- TOM20 (red) antibodies. Representative images of more than 50 cells are shown. **g**, OGDH depletion, which does not affect the interaction between DLST and DLD, inhibits the binding of DLST to KAT2A. OGDH was depleted in U251 cells. Immunoprecipitation analyses with an anti-DLST antibody were followed by immunoblotting analyses with the indicated antibodies. Representative images of triplicate experiments are shown. **h**, **i**, The NLS of DLST is required for nuclear distribution of the α-KGDH complex. DLST was depleted from U87 cells, which were reconstituted with expression of wild-type rDLST or the rDLST(R224A/K226E) NLS mutant. **h**, Immunofluorescent staining was performed with an anti- DLST or anti-OGDH antibody. The mitochondria and nuclei were stained with an anti-Tom20 antibody (red) and DAPI (blue), respectively. **i**, Immunoblotting analyses were performed with the indicated antibodies. Mitochondrial COX IV and IDH2 and nuclear PCNA were used to show lack of mitochondrial contamination of nuclear fractions and loading controls. Representative images of triplicate experiments are shown.

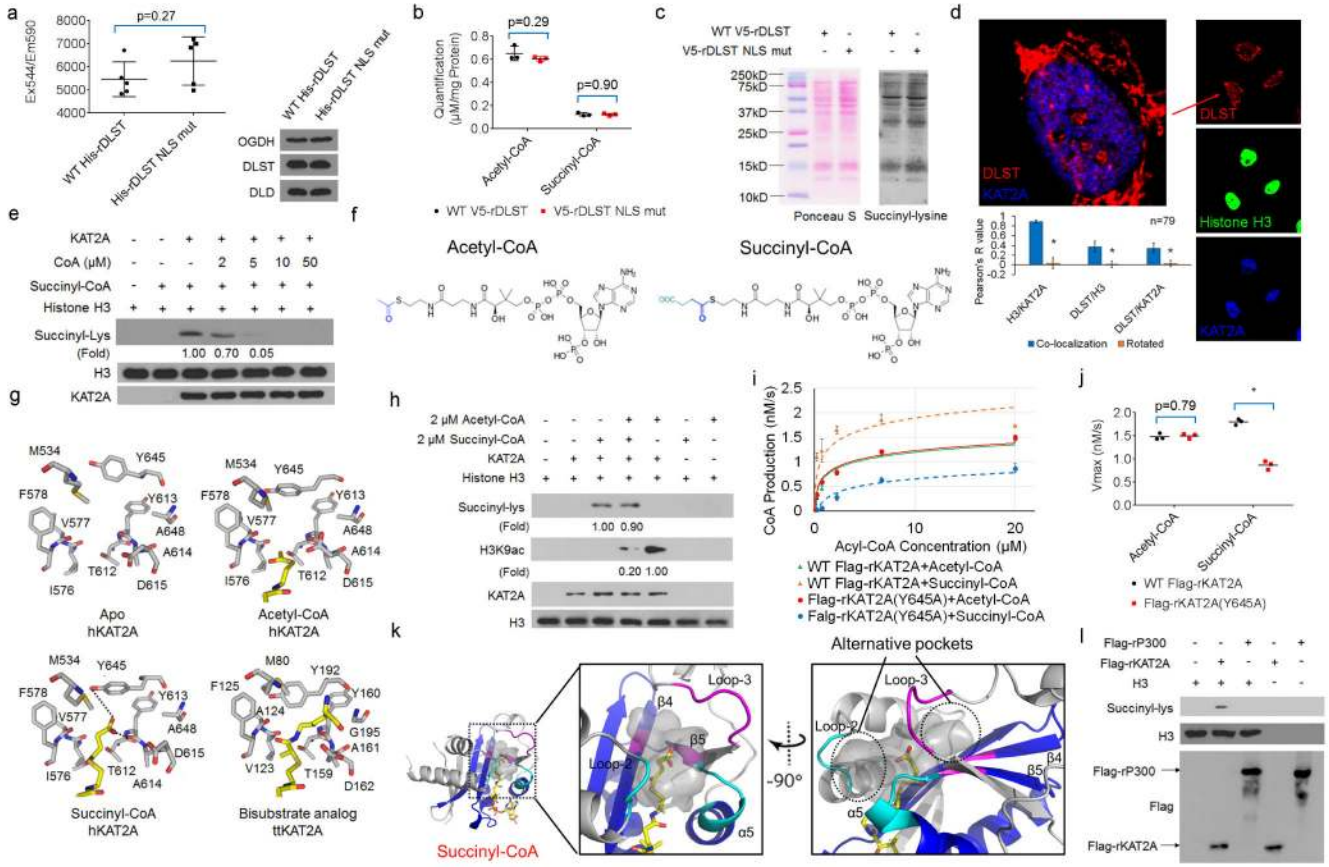

Extended Data Figure 2. KAT2A associates with α-KGDH and acts as a histone succinyltransferase

a, rDLST NLS mutation does not affect the enzymatic activity of α-KGDH. Wild-type His–rDLST or His–rDLST NLS mutant expressed in 293 cells was precipitated using Ni-NTA agarose beads. The enzymatic activity of α-KGDH was measured. Two-sided *t*-tests were conducted. The data are presented as the means ± s.d. from five independent experiments ($n = 5$). **b**, rDLST NLS mutant expression does not affect cellular levels of acetyl-CoA or succinyl-CoA. The levels of acetyl-CoA and succinyl-CoA in U251 cells with depleted endogenous DLST and reconstituted expression of wild-type V5–rDLST or V5–rDLST NLS mutant were measured by LC–MS/MS. Two-sided *t*-tests were conducted. The data are presented as the means ± s.d. from three independent experiments ($n = 3$). **c**, rDLST NLS mutant expression does not affect total cellular protein succinylation. Lysine succinylation of whole-cell lysate of U251 cells expressing wild-type V5–rDLST or V5–rDLST NLS mutant was analysed by immunoblotting analysis with an anti-succinyl-lysine antibody. The protein levels of each sample were shown by Ponceau S staining. Representative images of triplicate experiments are shown. **d**, Quantification of the colocalization of KAT2A, α-KGDH complex, and histone H3. Immunofluorescent analyses were performed with anti-DLST (red), anti-KAT2A (blue), and anti-histone H3 (green) antibodies. The Pearson's *R* value is used to present the extent of co-localization of two different targets. The random co-localization tests were conducted by 90° clockwise rotation of KAT2A (blue channel) and 180° clockwise rotation of histone H3 (green channel). Two-sided *t*-tests were conducted.

Statistical analysis for 79 individual cells ($n = 79$) was performed. * $P < 0.05$. **e**, KAT2A-mediated histone H3 succinylation is inhibited by CoA. KAT2A-mediated histone H3 succinylation was analysed by mixing purified KAT2A, histone H3, and succinyl-CoA (2 μM) with or without addition of the indicated concentrations of CoA. Representative images of triplicate experiments are shown. **f**, The chemical structures of acetyl-CoA and succinyl-CoA. The various acyl tail groups in acetyl-CoA and succinyl-CoA are highlighted in blue. **g**, Comparison of the structures of the catalytic domain of KAT2A in complex with different acyl-CoA ligands. The four structures shown from left to right are: apo structure of human KAT2A (this study), acetyl-CoA complex of human KAT2A (PDB ID 1Z4R), succinyl-CoA complex of human KAT2A (this study), and the bisubstrate analogue complex of *Tetrahymena thermophila* KAT2A (PDB ID 1M1D). For clarity, only residues surrounding the acyl groups are shown. The CoA substrate molecules are shown as yellow sticks. Hydrogen bonds are shown as dotted lines. **h**, KAT2A-mediated histone H3 succinylation is moderately affected by acetyl-CoA. KAT2A-mediated histone H3 succinylation was analysed by mixing purified KAT2A, histone H3, and succinyl-CoA (2 μM) with or without acetyl-CoA (2 μM). Immunoblotting analyses were performed with the indicated antibodies. Representative images of triplicate experiments are shown. **i**, **j**, The steady-state kinetics of KAT2A-mediated histone H3 modifications. Immunoprecipitated wild-type Flag–rKAT2A or Flag–rKAT2A(Y645A) from 293 cells was incubated with purified histone H3 in the presence of acetyl-CoA or succinyl-CoA. The steady-state kinetics of KAT2A activity was analysed by measuring CoA production. The K_m values of wild-type Flag– rKAT2A for histone H3 acetylation and succinylation were 0.83 ± 0.13 μM (means ± s.d.) and 0.36 ± 0.04 μM, respectively. The K_m values of Flag–rKAT2A(Y645A) for histone H3 acetylation and succinylation were 0.79 ± 0.08 μM and 1.73 ± 0.29 μM, respectively. The steady-state kinetic curves show the mean values from three independent measurements (**i**, $n = 3$). The V_{max} values of wild-type Flag–rKAT2A for histone H3 acetylation and succinylation were 1.56 ± 0.07 nM s^{-1} (mean ± s.d.) and 1.80 ± 0.06 nM s^{-1}, respectively. The V_{max} values of Flag–rKAT2A(Y645A) for histone H3 acetylation and succinylation were 1.50 ± 0.05 nM s^{-1} and 0.87 ± 0.09 nM s^{-1}, respectively (**j**). Two-sided *t*-tests were conducted. The data are presented as means ± s.d. from three independent experiments ($n = 3$). * $P < 0.05$. **k**, The KAT2A binding pocket for succinyl-CoA. The structurally conserved core regions of the HAT domains are shown in blue, whereas the flanking N- and C-terminal regions are shown in grey. The two enlarged panels, viewed with 90° rotation, display the van der Waals surface of KAT2A in grey around the succinyl group of succinyl-CoA. The cofactors are shown as follows: carbon in yellow, oxygen in red, nitrogen in blue, and sulfur in light brown. The alternative pockets are marked by dotted circles. The polypeptide regions surrounding the two extra pockets are highlighted in magenta and cyan, respectively. **l**, KAT2A, but not EP300, succinylates histone H3 *in vitro*. Purified histone H3 and succinyl-CoA were mixed with immunoprecipitated Flag–KAT2A or Flag–EP300 from 293 cells. Immunoblotting analyses were performed with the indicated antibodies. Representative images of triplicate experiments are shown.

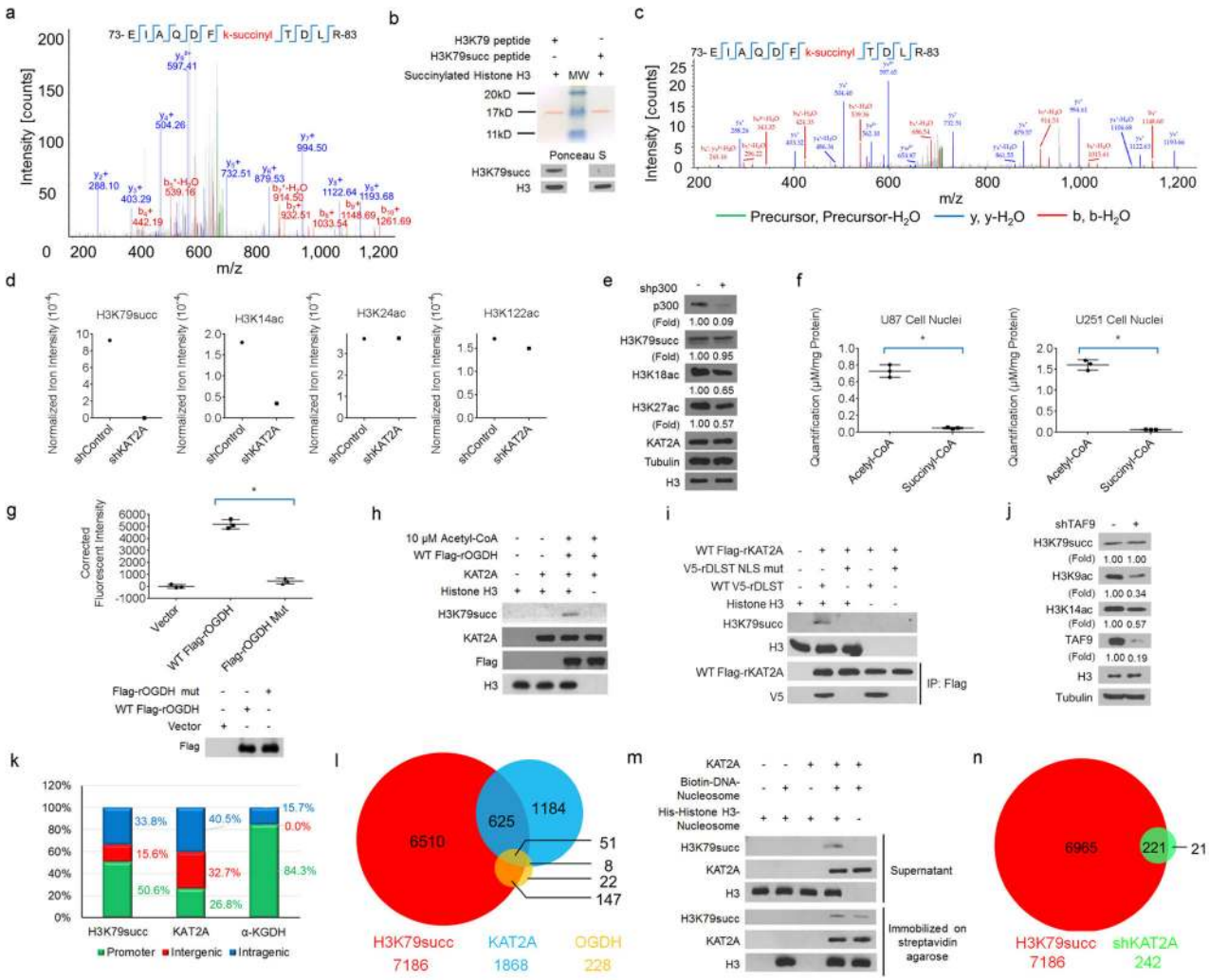

Extended Data Figure 3. KAT2A coupled with the α-KGDH complex regulates H3K79 succinylation and gene expression

a, H3K79 is succinylated. Purified wild-type or mutated histone H3 was incubated with purified KAT2A and succinyl-CoA. Mass spectrometric analysis of a tryptic fragment of histone H3 at monoisotopic *m*/*z* 718.35706 Da (+ 0.21 milli-mass unit (m.m.u.)/+ 0.29 p.p.m.) matched with the doubly charged peptide 73-EIAQDFKTDLR-83 with K7-succinyl (100.01604 Da), suggesting that H3K79 was succinylated. The IonScore (Mascot) was 51, and the expectation value (*P*) was 5.5×10^{-3}. **b**, Analyses of the specificity of the antibody against H3K79 succinylation. Synthetic histone H3 peptides with or without H3K79 succinylation were used to test the specificity of the antibody against H3K79 succinylation. Representative images of triplicate experiments are shown. MW, molecular weight. **c**, Identification of histone H3 K79 succinylation in U251 cells. Histones were extracted from U251 cells. Mass spectrometric analysis of a tryptic fragment of histone H3 extracts from U251 cells at monoisotopic *m*/*z* 718.35559 Da (– 1.26 m.m.u./ – 1.75 p.p.m.) matched with the doubly charged peptide 73-EIAQDFKTDLR-83 with K7-succinyl (100.01604 Da), suggesting that H3K79 was succinylated. The IonScore (Mascot) was 40, and the

expectation value (*P*) was 2.5×10^{-2}. **d**, Semi-quantitative comparison of posttranslational modifications of histone H3 with or without KAT2A depletion. Histones were extracted from U251 cells with or without KAT2A depletion. Mass spectrometric analyses identified the specific peptides of H3K14 acetylation (KSTGGKacAPR), H3K24 acetylation (KQLATKacAAR), H3K79 succinylation (EIAQDFKsuccTDLR), and H3K122 acetylation (RVTIMPKacDIQLAR). The succinylated H3K79 peptide was identified in the histone extracts from U251 cells in the absence but not presence of KAT2A depletion (Mascot IonScore, 40; expectation value, 2.5×10^{-2}). The peptides of H3K14ac, H3K24ac, and H3K122ac were identified in histone extracts from U251 cells with or without KAT2A depletion (Mascot IonScore > 30; expectation value < 0.05). KAT2A depletion reduced H3K14 acetylation, but not acetylation of H3K24 and H3K122. The semiquantitative results were obtained by the ratio of specific peptide iron intensity to total histone H3 iron intensity ($n = 1$). **e**, EP300 does not regulate histone H3 K79 succinylation. EP300 shRNA was expressed in U251 cells. Immunoblotting analyses were performed with the indicated antibodies. EP300 depletion reduced the acetylation of H3K18 and H3K27. Representative images of triplicate experiments are shown. **f**, Quantitative analyses of acetyl-CoA and succinyl-CoA levels in GBM cells. The levels of acetyl-CoA and succinyl-CoA in the nuclear extracts of U87 and U251 cells were measured by LC–MS/MS. Quantitative limits: ratio of signal intensity to noise intensity > 5. Two-sided *t*-tests were conducted. The data are presented as the means ± s.d. from three independent experiments ($n = 3$). * $P < 0.05$. **g**, The enzymatic activity of wild-type OGDH and inactive OGDH(P459A/ Y460A) was determined. Two-sided *t*-tests were conducted. The data are presented as the means ± s.d. from three independent experiments ($n = 3$). * $P < 0.05$. **h**, KAT2A uses α-KGDH-produced succinyl-CoA for histone H3 succinylation in the presence of acetyl-CoA and absence of exogenous succinyl-CoA. Purified KAT2A, histone H3, CoA, α-ketoglutarate, NAD^+, and acetyl-CoA were incubated with or without immunoprecipitated wild-type Flag–OGDH from 293 cells. Immunoblotting analyses were performed with the indicated antibodies. Representative images of triplicate experiments are shown. **i**, The DLST NLS mutant does not succinylate purified histone H3. Wild-type Flag–rKAT2A was coexpressed with wild-type V5–rDLST or V5–rDLST NLS mutant in 293 cells. The nuclei of 293 cells were extracted. Immunoprecipitated nuclear wild-type Flag–rKAT2A (which associated with wild-type V5–rDLST but not V5–rDLST NLS mutant) was incubated with purified histone H3, CoA, α-ketoglutarate, and NAD^+. Immunoblotting analyses were performed with the indicated antibodies. Representative images of triplicate experiments are shown. **j**, KAT2A in the SAGA complex does not regulate H3K79 succinylation. U251 cells with or without TAF9 shRNA were analysed by immunoblotting assay with the indicated antibodies. Representative images of triplicate experiments are shown. **k**, Genomic distributions of ChIP–seq peaks for H3K79 succinylation, KAT2A, and α-KGDH (OGDH) in U251 cells. **l**, Venn diagram shows the overlap of H3K79 succinylation (red)-, KAT2A (blue)-, and α-KGDH (yellow)- occupied gene promoters ($P = 0.02$ (one-sided Fisher's exact test)). **m**, H3K79 succinylation by KAT2A is a dynamic process. Purified KAT2A was incubated with streptavidin bead-immobilized nucleosomes and biotin-labelled DNA. The immobilized KAT2A–nucleosome complex was washed with PBS three times and incubated with succinyl-CoA in the presence or absence of purified and soluble nucleosome-containing His– histone H3, which was assembled with bacterially purified nonmodified histone

components. Immunoblotting analyses were performed with the indicated antibodies. Representative images of triplicate experiments are shown. **n**, KAT2A depletion reduces H3K79 succinylation in the gene promoter regions. Venn diagram showing the overlap of H3K79 succinylation-occupied gene promoters in U251 cells (red) and U251 cells expressing KAT2A shRNA (green) ($P = 0.02$ (one-sided Fisher's exact test)).

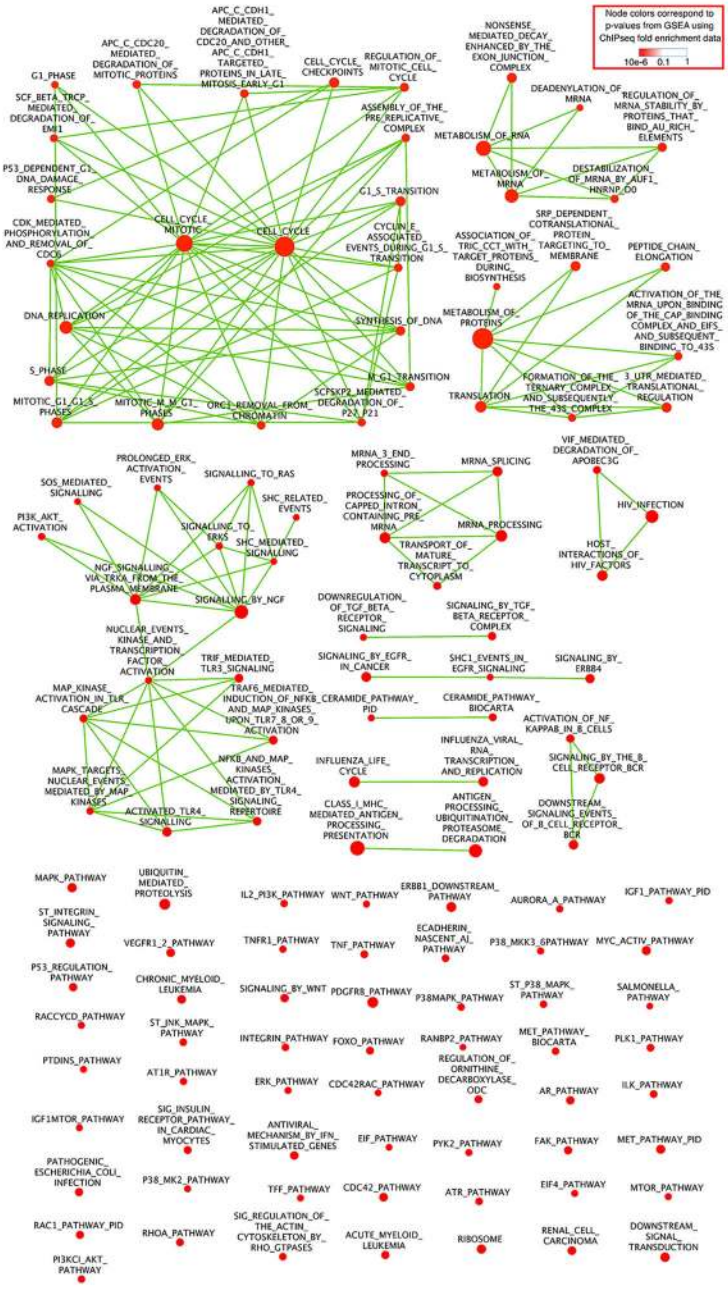

Extended Data Figure 4. Cell signalling pathways enriched with genes with H3K79-succinylated promoter regions

Nodes stand for 130 GSEA-identified pathways ($P < 0.005$ and FDR $q < 0.001$). Each node represents one pathway. The node size reflects the number of genes in the pathway, whereas

the node colour reflects the *P* value from the GSEA. Red indicates that the pathways are significantly enriched with genes with H3K79 succinylation in their promoter regions. Edges: two nodes are connected if the group of genes from the smaller node is strictly contained in the gene group from the larger node (that is, every member of the smaller pathway is also a member of the larger pathway). Highly connected node clusters reflect functional modules, which share a large portion of genes regulated by H3K79 succinylation. The 130 nodes are connected by 147 edges. Among the 130 nodes, 21 nodes, which are connected by 67 edges, are linked to the pathways of Cell Cycle and Cell Cycle Mitotic, both of which are defined in the Reactome database.

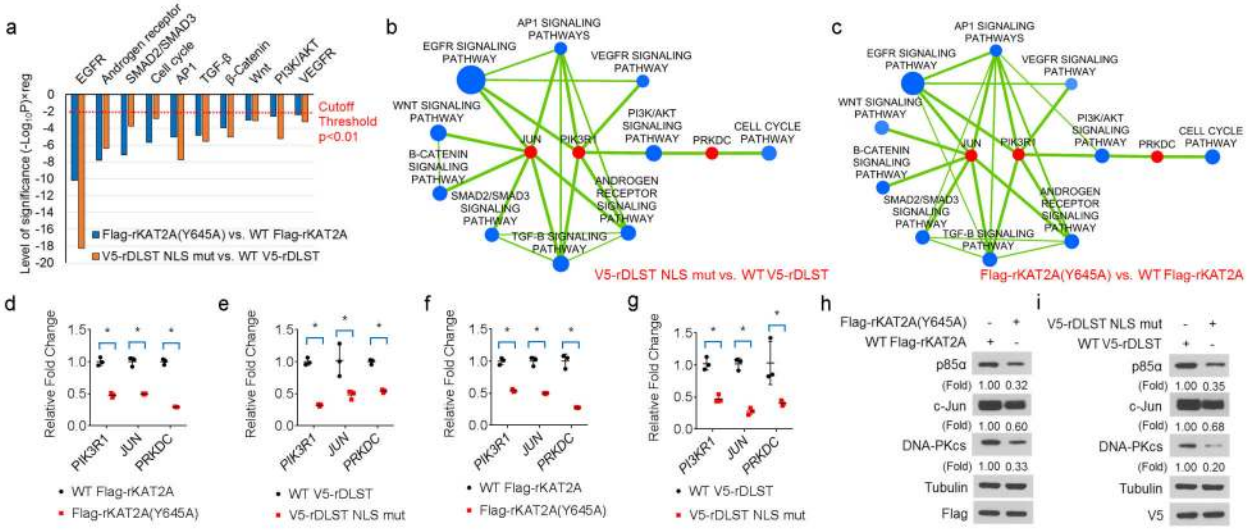

Extended Data Figure 5. Selected cell signalling pathways enriched with the genes with H3K79-succinylated promoter regions

a, H3K79 succinylation regulates critical cellular signalling pathways. Hypergeometric tests selected H3K79 succinylation-enriched signalling pathways in U251 cells with DLST(R224A/K226E) or KAT2A(Y645A) mutant expression. *y*-axis: level of significance from RNA-seq data, which takes the form of $(-\log_{10}P) \times \text{reg}$, where reg = − 1, indicating that the pathway is enriched with downregulated genes based on the comparison of mutant with wild-type proteins. One-sided hypergeometric test for overrepresentation was conducted. The data are from one RNA-seq sample. **b**, **c**, Combined view of ChIP–seq and RNA-seq data revealing histone H3K79 succinylation-enriched pathways that were significantly suppressed by the expression of V5–rDLST(R224A/K226E) (**b**) or Flag–rKAT2A(Y645A) (**c**). Significantly downregulated pathways were identified via hypergeometric tests (blue nodes, $P < 0.01$ and FDR $q < 0.05$) and were enriched with downregulated genes (individual genes with fold enrichment > 2 and FDR $q < 0.1$ in ChIP–seq data and $P < 0.05$ and FDR $q < 0.1$ in RNA-seq data). The selected genes (*PRKDC*, *JUN*, and *PIK3R1*) were those that were most significantly suppressed (red nodes, $P < 0.005$ and FDR $q < 0.05$ in RNA-seq; fold enrichment > 4 and FDR $q < 0.05$ in ChIP–seq) or important hitches between these suppressed pathways. The blue node size reflects the number of significantly suppressed genes in the pathway. Edges represent more than 40% of gene members shared between the pathways. **d**, **e**, α-KGDH-coupled KAT2A regulates gene

expression. mRNA expression levels of *PIK3R1*, *JUN*, and *PRKDC* in U87 cells with depleted endogenous KAT2A and reconstituted expression of wild-type Flag–rKAT2A or Flag–rKAT2A(Y645A) mutant (**d**) or with depleted endogenous DLST and reconstituted expression of wild-type V5–rDLST or V5–rDLST NLS mutant (**e**) were determined using quantitative PCR. Two-sided *t*-tests were conducted. The data are presented as the means ± s.d. from three independent experiments ($n = 3$). * $P < 0.05$. **f**, **g**, α-KGDH-coupled KAT2A regulates gene expression. mRNA expression levels of *PIK3R1*, *JUN*, and *PRKDC* in U251 cells with depleted endogenous KAT2A and reconstituted expression of wild-type Flag–rKAT2A or Flag–rKAT2A(Y645A) (**f**) or with depleted endogenous DLST and reconstituted expression of wild-type V5–rDLST or V5–rDLST NLS mutant (**g**) were determined using quantitative PCR. Two-sided *t*-tests were conducted. The data are presented as the means ± s.d. from three independent experiments ($n = 3$). * $P < 0.05$. **h**, **i**, α-KGDH-coupled KAT2A regulates gene expression. Expression levels of p85α, c-Jun, and DNA-PKcs in U251 cells with depleted endogenous KAT2A and reconstituted expression of wild-type Flag– rKAT2A or Flag–rKAT2A(Y645A) (**h**) or with depleted endogenous DLST and reconstituted expression of wild-type V5–rDLST or V5–rDLST NLS mutant (**i**) were determined using immunoblotting analyses with the indicated antibodies. Representative images of triplicate experiments are shown.

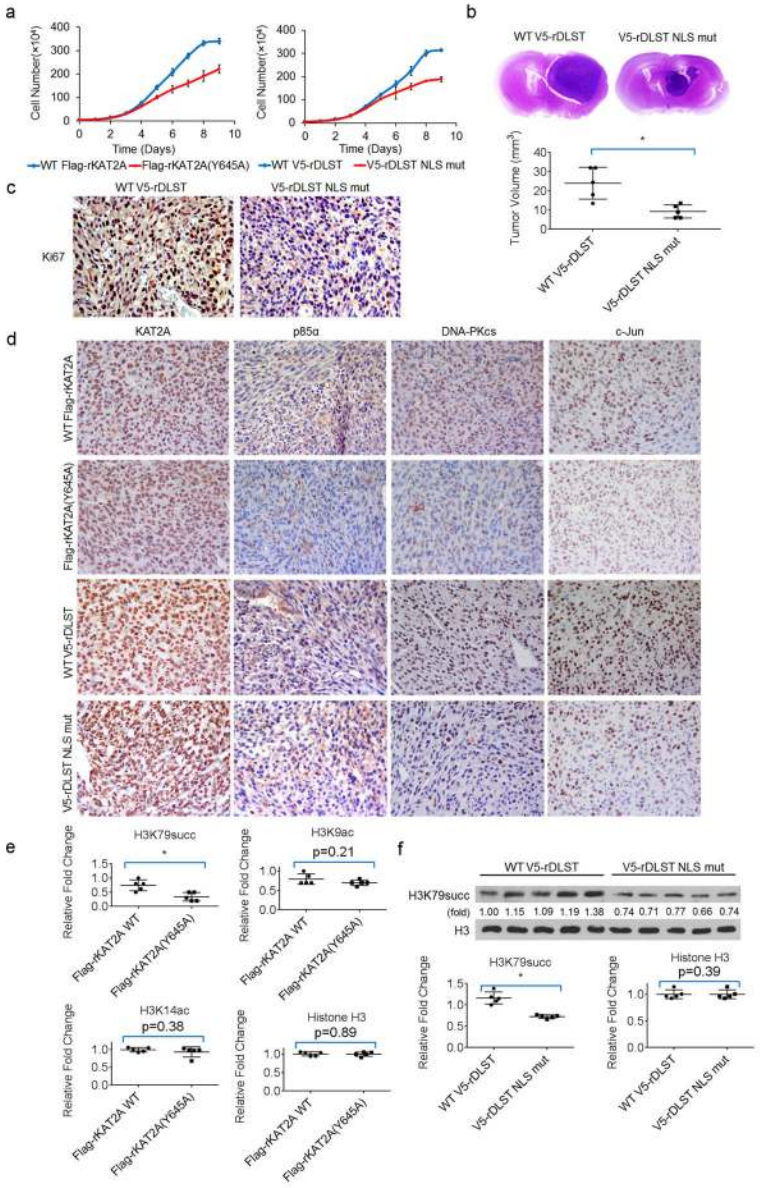

Extended Data Figure 6. α-KGDH-coupled KAT2A promotes tumour growth

a, α-KGDH-coupled KAT2A promotes tumour cell proliferation. A total of 10^4 U251 cells with depleted endogenous KAT2A and reconstituted expression of wild-type Flag–rKAT2A or Flag–rKAT2A(Y645A) or depleted endogenous DLST and reconstituted expression of wild-type V5–rDLST or V5–rDLST NLS mutant were plated. The cells were collected and counted daily for nine days. The data are presented as the means ± s.d. from three independent experiments ($n = 3$). **b**, α-KGDH-coupled KAT2A promotes tumour growth. U87 cells with depleted endogenous DLST and reconstituted expression of wild-type V5–rDLST or V5–rDLST NLS mutant were intracranially injected into athymic nude mice. Representative haematoxylin and eosin-stained coronal brain sections are shown. Tumour volumes were calculated. Two-sided *t*-tests were conducted. Data represent the means ± s.d. of 5 mice ($n = 5$). * $P < 0.05$. **c**, Immunohistochemical analyses of the brain tumour sections

were performed with an anti-Ki67 antibody. **d**, Immunohistochemical analyses of the brain tumour sections were performed with the indicated antibodies. **e**, **f**, α-KGDH-coupled KAT2A promotes H3K79 succinylation in tumour cells. Quantification of the immunoblotting (Fig. 4d) was performed using ImageJ software (**e**). Immunoblotting analyses of histone extracts from tumour tissues were performed with the indicated antibodies (**f**). Two-sided *t*-tests were conducted. Quantitative data represent the means ± s.d. of 5 samples ($n = 5$). * $P < 0.05$. Representative images of triplicate experiments are shown.

Extended Data Table 1

Collection and refinement statistics of co-crystal structures

	Apo (PDB ID: 5TRM)	succinyl-CoA complex (PDB ID: 5TRL)
Data collection		
Space group	P41212	P213
Cell dimensions		
a, *b*, *c* (Å)	173.474, 173.474, 347.637	175.728, 175.728, 175.728
α, *β*, *γ* (°)	90, 90, 90	90, 90, 90
Resolution (Å)	50-2.9 (2.95-2.9)	50-2.3 (2.34-2.3)
R_{merge}	12.0 (56.1)	14.6 (99.8)
$I/\sigma(I)$	15.1 (2.7)	28.1 (2.4)
Completeness (%)	99.7 (100)	100 (99.9)
Redundancy	6.2 (5.6)	21.5 (12.8)
Refinement		
Resolution (Å)	48.2-2.90 (2.93-2.90)	30.1-2.30 (2.33-2.30)
Unique reflections	117236 (11588)	80101 (7952)
R_{work}/R_{free}	21.5/27.3	19.7/21.3
No. atoms		
Protein	31738	10537
Ligand/ion	N/A	440 (succinyl-CoA)
(specify/describe)		
Water	N/A	599
B factors		
Protein	32.53	34.03
Ligand/ion	N/A	43.85
Water	N/A	39.93
R.m.s. deviations		
Bond lengths (Å)	0.009	0.004
Bond angles (°)	0.867	0.776

One crystal was used for each structure. Values in parentheses are for highest-resolution shell.

Supplementary Material

Refer to Web version on PubMed Central for supplementary material.

Acknowledgments

We thank L. Li at the University of Texas Health Science at Houston for technical support and D. Norwood and T. Locke for critical reading of this manuscript. This work was supported by National Institute of Neurological Disorders and Stroke grant R01 NS089754 (Z.L.), National Cancer Institute grants 2R01 CA109035 (Z.L.), R01 CA169603 (Z.L.), MD Anderson Support Grant P30CA016672, Welch Foundation grant C-1565 (Y.J.T.), and the National Institutes of Health Brain Cancer Specialized Program of Research Excellence (2P50 CA127001). Z.L. is a Ruby E. Rutherford Distinguished Professor.

References

1. Weinert BT, et al. Lysine succinylation is a frequently occurring modification in prokaryotes and eukaryotes and extensively overlaps with acetylation. Cell Reports. 2013; 4:842–851. [PubMed: 23954790]
2. Zhang Z, et al. Identification of lysine succinylation as a new post-translational modification. Nat Chem Biol. 2011; 7:58–63. [PubMed: 21151122]
3. Yang W, et al. Nuclear PKM2 regulates β-catenin transactivation upon EGFR activation. Nature. 2011; 480:118–122. [PubMed: 22056988]
4. Jiang Y, et al. Local generation of fumarate promotes DNA repair through inhibition of histone H3 demethylation. Nat Cell Biol. 2015; 17:1158–1168. [PubMed: 26237645]
5. Sutendra G, et al. A nuclear pyruvate dehydrogenase complex is important for the generation of acetyl-CoA and histone acetylation. Cell. 2014; 158:84–97. [PubMed: 24995980]
6. Wang L, Dent SY. Functions of SAGA in development and disease. Epigenomics. 2014; 6:329–339. [PubMed: 25111486]
7. Grant PA, et al. Yeast Gcn5 functions in two multisubunit complexes to acetylate nucleosomal histones: characterization of an Ada complex and the SAGA (Spt/Ada) complex. Genes Dev. 1997; 11:1640–1650. [PubMed: 9224714]
8. Nguyen Ba AN, Pogoutse A, Provart N, Moses AM. NLStradamus: a simple Hidden Markov Model for nuclear localization signal prediction. BMC Bioinformatics. 2009; 10:202. [PubMed: 19563654]
9. Schuetz A, et al. Crystal structure of a binary complex between human GCN5 histone acetyltransferase domain and acetyl coenzyme A. Proteins. 2007; 68:403–407. [PubMed: 17410582]
10. Lin Y, Fletcher CM, Zhou J, Allis CD, Wagner G. Solution structure of the catalytic domain of GCN5 histone acetyltransferase bound to coenzyme A. Nature. 1999; 400:86–89. [PubMed: 10403255]
11. Clements A, et al. Structural basis for histone and phosphohistone binding by the GCN5 histone acetyltransferase. Mol Cell. 2003; 12:461–473. [PubMed: 14536085]
12. Poux AN, Marmorstein R. Molecular basis for Gcn5/PCAF histone acetyltransferase selectivity for histone and nonhistone substrates. Biochemistry. 2003; 42:14366–14374. [PubMed: 14661947]
13. Poux AN, Cebrat M, Kim CM, Cole PA, Marmorstein R. Structure of the GCN5 histone acetyltransferase bound to a bisubstrate inhibitor. Proc Natl Acad Sci USA. 2002; 99:14065–14070. [PubMed: 12391296]
14. Ringel AE, Wolberger C. Structural basis for acyl-group discrimination by human Gcn5L2. Acta Crystallogr D. 2016; 72:841–848.
15. Dyda F, Klein DC, Hickman AB. GCN5-related N-acetyltransferases: a structural overview. Annu Rev Biophys Biomol Struct. 2000; 29:81–103. [PubMed: 10940244]
16. Kaczmarska Z, et al. Structure of p300 in complex with acyl-CoA variants. Nat Chem Biol. 2017; 13:21–29. [PubMed: 27820805]
17. Adams PD, et al. PHENIX: a comprehensive Python-based system for macromolecular structure solution. Acta Crystallogr D. 2010; 66:213–221. [PubMed: 20124702]
18. Emsley P, Lohkamp B, Scott WG, Cowtan K. Features and development of Coot. Acta CrystallogrD. 2010; 66:486–501.

19. Subramanian A, et al. Gene set enrichment analysis: a knowledge-based approach for interpreting genome-wide expression profiles. Proc Natl Acad Sci USA. 2005; 102:15545–15550. [PubMed: 16199517]

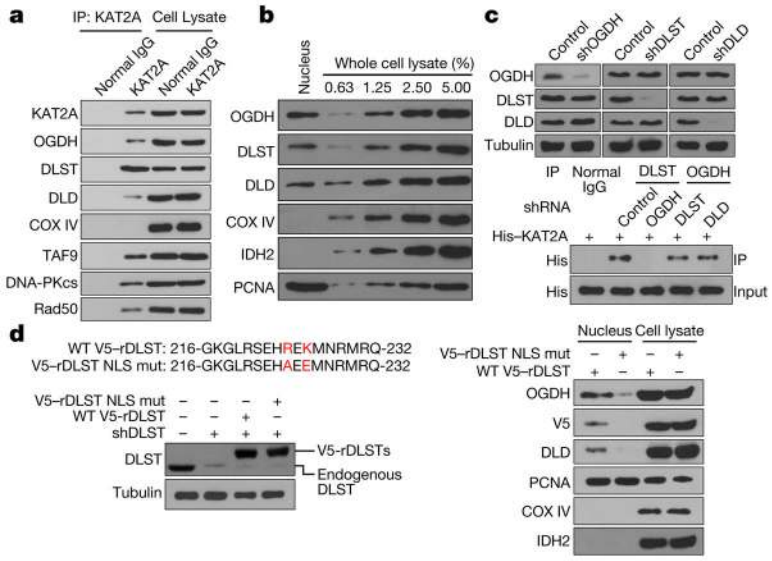

Figure 1. KAT2A interacts with the α-KGDH complex in the nucleus

a–**d**, Immunoblotting analyses were performed with the indicated antibodies. Representative images of triplicate experiments are shown. **a**, KAT2A binds to the α-KGDH complex. Immunoprecipitation analyses of U251 cells with an anti-KAT2A antibody were performed. KAT2A-associated proteins were analysed by immunoblotting. **b**, Nuclear localization of α-KGDH. Immunoblotting analyses of α-KGDH subunits in extracted nuclei of U251 cells were performed. **c**, OGDH binds to KAT2A. The α-KGDH complex in U251 cells with or without depletion of OGDH, DLST, or DLD using short hairpin RNA (shOGDH, shDLST or shDLD, respectively) was immunoprecipitated with the indicated antibodies and incubated with bacterially purified full-length His–KAT2A protein. **d**, DLST is required for nuclear distribution of the α-KGDH complex. DLST was depleted from U251 cells, which were reconstituted with expression of RNA interference-resistant (r) wild-type (WT) V5–rDLST or V5–rDLST(R224A/K226E) mutant (V5–rDLST NLS mut). Immunoblotting analyses were performed. Mitochondrial COX IV and IDH2 and nuclear proliferating cell nuclear antigen (PCNA) were used as controls.

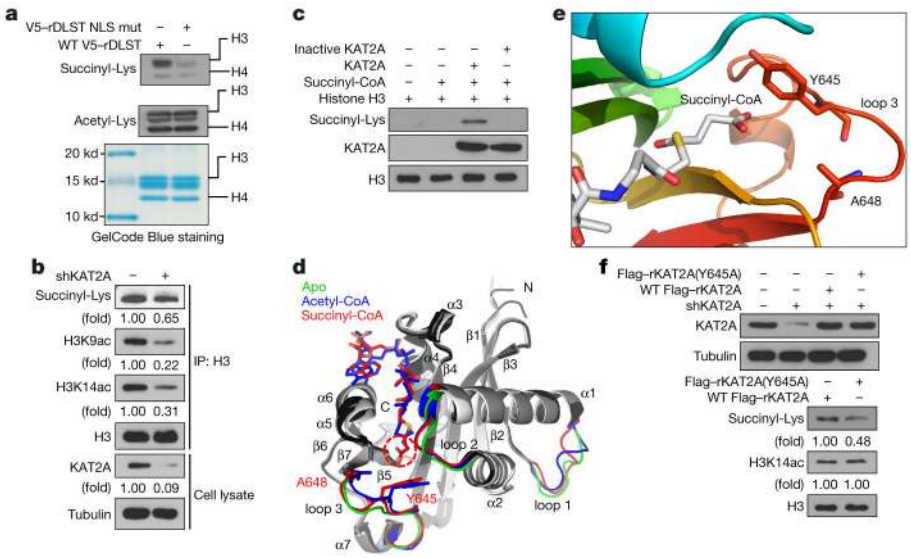

Figure 2. KAT2A acts as a histone succinyltransferase

a–**c**, **f**, Immunoblotting analyses were performed with the indicated antibodies. Representative images of triplicate experiments are shown. **a**, Nuclear DLST promotes histone H3 succinylation. Histones were extracted from U251 cells with depleted endogenous DLST and reconstituted expression of wild-type rDLST or the rDLST NLS mutant. The total histone acetylation and succinylation levels were analysed. The histone protein levels were analysed with GelCode Blue staining. **b**, KAT2A regulates histone H3 succinylation. Histone H3 proteins were immunoprecipitated from U251 cells with or without KAT2A depletion (by shRNA). **c**, KAT2A succinylates histone H3. KAT2A-mediated histone H3 succinylation was analysed by mixing purified KAT2A, histone H3, and succinyl-CoA. Heat-inactived KAT2A was used as a negative control. **d**, Superimposition of the KAT2A apo, KAT2A–succidnyl-CoA complex, and KAT2A–acetyl-CoA complex structures. Models show KAT2A in ribbons, succinyl-CoA in red sticks, and acetyl-CoA in blue sticks. The three loop regions are highlighted, with the apo structure in green, KAT2A–acetyl-CoA complex in blue, and KAT2A–succinyl-CoA complex in red. The rest of the structures are shown in white, grey, and black for apo, the KAT2A-acetyl–CoA complex, and the KAT2A-succinyl–CoA complex, respectively. The three loops, secondary structure elements, and the N and C termini of KAT2A are labelled. The two extra carbons in the succinyl group compared to the acetyl group are highlighted with red dashes. **e**, Interactions between succinyl-CoA and loop 3 of KAT2A. KAT2A is rainbow-coloured, with the N terminus in blue and the C terminus in red. Tyr645, Ala648, and the succinyl-CoA molecule are shown as sticks. **f**, KAT2A Y645 is critical for histone H3 succinylation. U251 cells with depleted endogenous KAT2A and reconstituted expression of wild-type Flag–rKAT2A or Flag–rKAT2A(Y645A) were analysed by immunoblotting assay.

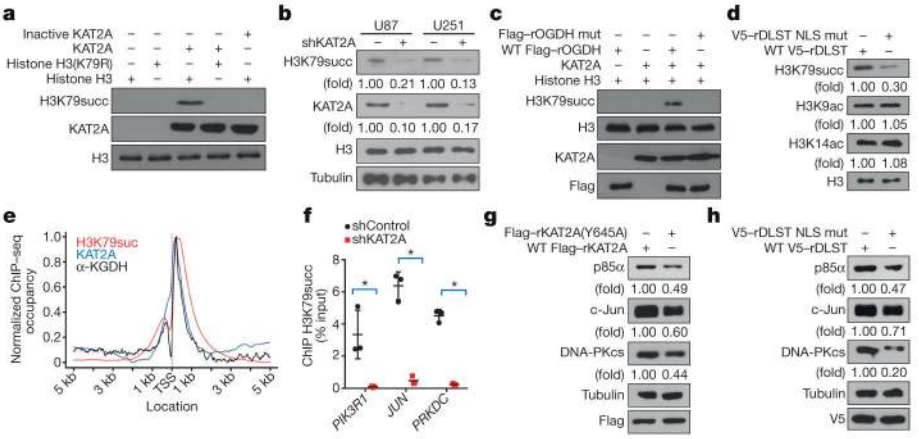

Figure 3. α-KGDH-coupled KAT2A regulates H3K79 succinylation and gene expression

a–**d**, **g**, **h**, Immunoblotting analyses were performed with the indicated antibodies. Representative images of triplicate experiments are shown. **a**, H3K79 is succinylated. Purified wild-type histone H3 or H3(K79R) was incubated with succinyl-CoA and purified wild-type or inactive KAT2A. **b**, KAT2A-depdendent H3K79 succinylation. KAT2A shRNA was expressed in U87 and U251 cells. **c**, α-KGDH provides succinyl-CoA for H3K79 succinylation. Purified KAT2A, histone H3, CoA, α-ketoglutarate, and NAD^+ were incubated with or without immunoprecipitated wild-type Flag–rOGDH or Flag–rOGDH(P459A/Y460A) from 293 cells. Mut, mutant. **d**, Nuclear localization of α-KGDH is involved in H3K79 succinylation. U251 cells with depleted endogenous DLST and reconstituted wild-type V5–rDLST or V5–rDLST NLS mutant were analysed by immunoblotting assay. **e**, Average genome-wide occupancies of H3K79 succinylation (red), KAT2A (blue), and α-KGDH (OGDH, black) around the transcription start site (TSS). **f**, KAT2A promotes H3K79 succinylation at the indicated gene promoters. ChIP assay with an anti-H3K79 succinylation antibody and quantitative PCR with primers against the promoter regions of *PIK3R1*, *JUN*, and *PRKDC* in U251 cells with or without KAT2A depletion were performed. Two-sided *t*-test analyses were conducted. The data are presented as the means ± s.d. of three independent experiments ($n = 3$). * $P < 0.05$. **g**, **h**, α-KGDH-coupled KAT2A regulates gene expression. Protein expression levels of PIK3R1, JUN, and PRKDC in U87 cells with depleted endogenous KAT2A and reconstituted expression of wild-type Flag–rKAT2A or Flag–rKAT2A(Y645A) (**g**) or with depleted endogenous DLST and reconstituted expression of wild-type V5–rDLST or V5–rDLST NLS mutant (**h**) were determined by immunoblotting analyses.

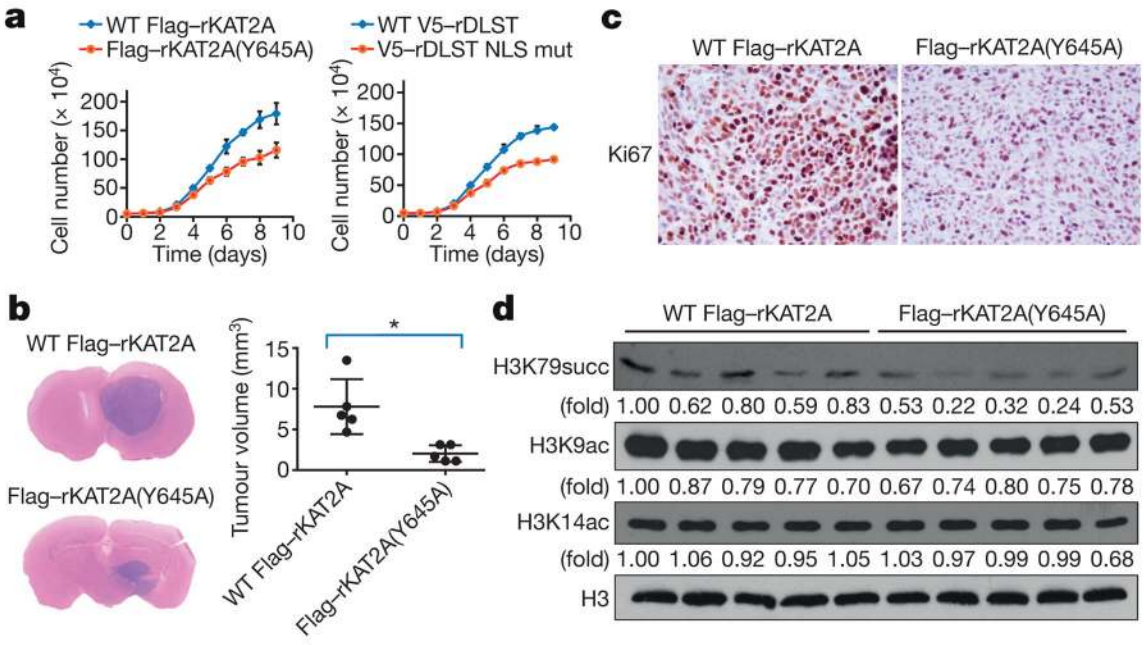

Figure 4. H3K79 succinylation by α-KGDH-coupled KAT2A promotes tumour growth

a, α-KGDH-coupled KAT2A promotes tumour cell proliferation. U87 cells with depleted endogenous KAT2A and reconstituted expression of wild-type Flag–rKAT2A or Flag–rKAT2A(Y645A) or depleted endogenous DLST and reconstituted expression of wild-typeV5–rDLST or V5–rDLST NLS mutant were plated. The cells were collected and counted daily for 9 days. The data are presented as the means ± s.d. from three independent experiments ($n = 3$). **b**, α-KGDH-coupled KAT2A promotes tumour growth. U87 cells, with depleted endogenous KAT2A and reconstituted expression of wild-type Flag–rKAT2A or Flag–rKAT2A(Y645A), were injected intracranially into athymic nude mice. Haematoxylin and eosin-stained coronal brain sections (representative of five brains) are shown. Tumour volumes were calculated. Two-sided *t*-test analyses were conducted. Data represent the means ± s.d. of five mice ($n = 5$). * $P < 0.05$. **c**, Immunohistochemical analyses of the indicated brain tumour sections were performed with an anti-Ki67 antibody. The images represent the results of five tissue slides. **d**, α-KGDH-coupled KAT2A promotes H3K79 succinylation in tumour cells. Immunoblotting analyses of the histone extracts from tumour tissues were performed with the indicated antibodies. Representative images of triplicate experiments are shown.